3-6-2006

Modeling E & F Region Ionospheric Response to X-Ray Solar Flares

Annette M. Parsons

Modeling E & F Region Ionospheric
Response to X-Ray Solar Flares

THESIS

Annette M. Parsons, 1st Lieutenant, USAF
AFIT/GAP/ENP/06-14

DEPARTMENT OF THE AIR FORCE
AIR UNIVERSITY

AIR FORCE INSTITUTE OF TECHNOLOGY

Wright-Patterson Air Force Base, Ohio

The views expressed in this thesis are those of the author and do not reflect the official policy or position of the United States Air Force, Department of Defense, or the United States Government.

AFIT/GAP/ENP/06-14

Modeling E & F Region Ionospheric Response to X-Ray Solar Flares

THESIS

Presented to the Faculty

Department of Engineering Physics

Graduate School of Engineering and Management

Air Force Institute of Technology

Air University

Air Education and Training Command

In Partial Fulfillment of the Requirements for the

Degree of Master of Science (Applied Physics)

Annette M. Parsons, BS

1st Lieutenant, USAF

March 2006

AFIT/GAP/ENP/06-14

Modeling E & F Region Ionospheric
Response to X-Ray Solar Flares

Annette M. Parsons, BS
1st Lieutenant, USAF

Approved:

Christopher G. Smithtro (Chairman)	6 Mar 06 date
David W. Gerts (Member)	6 Mar 06 date
Thomas A. Niday (Member)	6 Mar 06 date

Abstract

This research takes an existing ionospheric model and modifies it to include the effects of solar flare activity. Solar flares are a localized explosive release of magnetic energy that appears as a sudden, short-lived brightening in the sun's chromosphere. This additional energy is deposited in the earth's ionosphere, temporarily changing its properties, which can affect military communications. Studying the effects of moderate solar flares will improve our understanding of the ionosphere's response, leading to better operational models. Modification of the model is accomplished by adding a flare irradiance model to represent solar irradiance changes due to a flare. The irradiance output is then used to calculate the photoionization rates, electron impact ionization rates, and electron heating rates in the ionospheric model. After the results of this integration are validated, two moderate flares are modeled and then compared to ionospheric measurements from Bear Lake Observatory. It is found that the new model is able to accurately reflect the response of the E and lower F region of the ionosphere, but above the F_2 peak the electron temperature does not increase as initially expected. Future work will need to resolve this discrepancy so that the model can accurately develop the ionosphere's response to solar flares.

Acknowledgments

I would like to express my sincere appreciation to my faculty advisor and sponsor, Maj. Christopher Smithtro for his guidance and support throughout this thesis effort. The infinitely large amount of work he provided me ensured that I was gainfully employed day and night. Through all this I certainly appreciated his insight and experience but mostly I am grateful for his patience with my countless number of questions and several clueless moments.

I am also grateful to Dr Robert Schunk and Michael David from the Physics Department of Utah State University for their support and assistance in using and understanding the TDIM model. I would also like to thank Phil Chamberlain from Colorado State University for providing flare irradiance data from his FISM model.

Finally, but most importantly, I would like to thank my husband and my three children for their patience, support and the full time use of the family's computer.

Annette M. Parsons

Table of Contents

Page

List of Figures

Figure Page

List of Tables

Modeling E & F Region Ionospheric
Response to X-Ray Solar Flares

I. Introduction

Many current military applications must account for the effects of the solar-terrestrial environment in their design and operation. For instance, communication applications often rely on signals reflecting from the ionosphere to propagate signals from sender to receiver. Changes in the reflective properties of the ionosphere, due to increased solar activity, can significantly alter a signal's propagation path. Another area of concern is the effect of the space environment on satellites. While this environment is inherently hazardous to satellites, an increase in solar activity can decrease a satellites projected lifetime by years. Degradation in the satellites orbit, anomalous incidents, and even spacecraft failures have been recorded during increased solar activity. Hence, it is imperative that military operators have accurate forecasts for the state of the ionosphere and the space environment. This would allow them to plan and prepare accordingly to avoid detriment to military operations.

There are many atmospheric models that have been developed to be used in space weather operations. These models do not have an inherent capability to model solar flare[1] events, decreasing the utility of the space weather forecast for the operator. One

[1] A solar flare is a localized explosive release of magnetic energy that appears as a sudden, short-lived brightening of an area in the sun's chromosphere, see section 2.1.

such model is the Time-Dependent Ionospheric Model (TDIM), developed at Utah State University [*Schunk*, 1988]. This model accurately reflects the quiet (non-flare) E and F regions of the ionosphere[2] but lacks the ability to reproduce the effects of a sudden change from a solar flare. What I hope to accomplish with this thesis is an improved understanding of the ionospheric response to solar flares in order to improve operational model output.

This area of research will modify the modeling techniques used to model the E and F regions of the ionosphere in the TDIM to include the effects of moderate solar x-ray flare activity. This model has two significant short-falls that will need to be corrected in order for it to accurately reproduce the ionospheric response to a solar flare. The first is the model's inability to update the solar irradiance during a solar flare and the second is that it does not self-consistently include the effect of photoelectrons. These inputs are important in the proper development of the ionospheric response to a solar flare. Once these shortfalls have been corrected it is hoped that a realistic ionospheric response will be generated.

Once this model is rigorously proven to accurately reproduce the effects of flares on the ionosphere, the model can be run and the data analyzed for all magnitudes of M-class flares. These results can then be used operationally to forecast the impact of a flare on the ionosphere. This will be done in real time as the flare occurs since there is currently no way to forecast a solar flare event. This can then be translated to the customer to include what frequencies will be affected over a given period of time.

[2] The E and F region altitudes vary but generally the E region is from 100 to 150 km and the F region is from 150 to 350 km, see section 2.2.

The following chapters will provide a background, show the model development, explain the results and discuss conclusions and future work. Chapter 2 will discuss the required background knowledge to understand this work. We will start by discussing solar flares, the ionosphere, solar irradiance, electron temperature, density and heating, ionograms, previous work, and models used in the research. In Chapter 3 a discussion of the methodology used to modify the ionospheric model will comprise the majority of the chapter. Section 3.2 will also discuss ionograms from Bear Lake Observatory that are used to compare to the modeled data. Chapter 4 will analyze the results from two modeled flares; comparing the results to the real data. And finally, Chapter 5 will end with the final conclusions of the research and what future work may take place.

II. Background

Space weather is a relatively new research area which involves the complicated interactions between the sun and the earth. The National Space Weather Program, which began in 1994, defines space weather as "...conditions on the sun and in the solar wind, magnetosphere, ionosphere, and thermosphere that can influence the performance and reliability of space-borne and ground-based technological systems and can endanger human life or health. Adverse conditions in the space environment can cause disruption of satellite operations, communications, navigation, and electric power distribution grids, leading to a variety of socioeconomic losses" [*NSWP Strategic Plan*, 1995]. This is a broad area to discuss, so we will briefly examine what is relevant to this research in the following sections.

2.1 Solar Flares

A solar flare is a localized explosive release of magnetic energy that appears as a sudden, short-lived brightening of an area in the sun's chromosphere. This energy is released through a process called magnetic reconnection and is on the order of 10^{21} to 10^{25} J. The energy is released mainly in the form of electromagnetic radiation and energetic particles. There is a significant increase in the extreme ultra violet (EUV)[3] and X-ray regions of the solar output but the total solar output increase is less than 0.01% [*Foukal*, 2004]. It is this increase in EUV and x-ray intensities that will drive changes in the ionosphere.

[3] In this paper EUV is defined from 5-105 nm.

The increased intensities are use to classify flares in two ways. First the flare's maximum area as observed in the Hα line and second by the soft x-ray classification. Flares in this paper will be categorized according to the x-ray classification scheme as defined in Table 1. Importance is designated by a letter followed by a number multiplier: i.e. M4.2 indicates a peak flux of 4.2 x 10^{-5} Wm^{-2}.

Table 1. X-Ray flare classification.

Importance	Peak Flux in 0.1-0.8 nm range (Wm^{-2})
B	10^{-7}
C	10^{-6}
M	10^{-5}
X	10^{-4}

2.2 The Ionosphere

The ionosphere is the region of the atmosphere that contains significant numbers of electrons and ions, generally considered to be at altitudes above ~60 km. This region is sensitive to the sun's x-ray and ultraviolet radiation output, which ionizes the neutral particles. Once these electrons and ions are formed, they are affected by chemical reactions, diffusion, wave disturbances, plasma instabilities and transport due to electric and magnetic fields [*Schunk*, Chap. 1, 2000]. Figure 1 is an example of a typical profile of electron density of the Earth's ionosphere at solar minimum versus maximum and nighttime versus daytime.

In Figure 1, you can see four defined regions in the ionosphere; the D, E, F_1, and F_2 regions. Since at night the photoionization process stops, the overall electron density

will drop throughout the ionosphere, with the greatest loss in the F region. The D and F_1 region peaks will disappear so that there are only two defined regions at night: the E and F_2 regions. The E region has a definable peak with its electron density maintained through photoionization by starlight, moonlight, and scattered sunlight. The F_2 region maintains a definable peak also, with its electron density maintained through transport and diffusion processes. During solar maximum, electron densities will increase due to an increase in the flux of EUV and x ray photons.

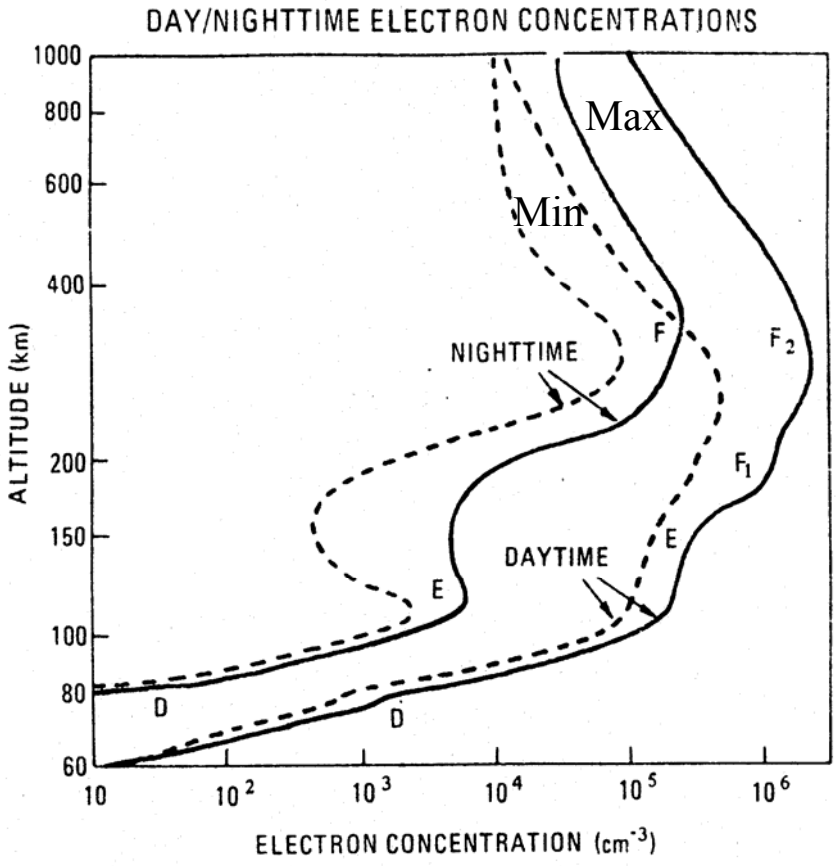

Figure 1. The electron density profile of Earth's atmosphere plotted as a function of altitude for solar minimum (dashed) vs. maximum (solid), and nighttime vs. daytime.

There are specific wavelength ranges that are responsible for ionizing each region. In the D region the primary source of ionization is by solar x-ray (0.2 to 0.8 nm) ionization of N_2 and O_2, and Lyman-α (121.1 nm) ionization of NO. The regions concerned with in this paper are the E and F regions, where primary ionization of the E region is caused by the 5 to 10 nm and 95 to 105 nm wavelengths. Here the resulting major ions are O_2^+ and NO^+. The F_1 region is ionized at the 91 nm wavelength which creates the region's principle ion, O^+. Finally the F_2 region's major ion is also O^+ with a density peak between 200 and 400 km. Formation of this region is the result of a balance between plasma transport and chemical loss processes. These regions of the ionosphere are impacted during a solar flare event because of the particular wavelengths that are enhanced during a solar flare.

In a solar flare there is an increase in solar flux. It is this increase in solar flux that directly impacts the daytime midlatitude ionosphere. Increases in intensity in the x-ray and EUV part of the electromagnetic spectrum will increase photoionization rates and enhance the temperature of the plasma in the ionosphere. In flares that are very large, greater than X10, the increased photoionization rates will cause the total electron count (TEC) and the F_2 peak electron density (N_mF_2) to increase by up to 20% and decrease the height of the maximum electron density (H_mF_2) peak by 20% [*Huba et al.*, 2005]. While *Smithtro et al*. [2004] has shown a 10% decrease in the peak F_2 frequency (f_oF_2) for certain M class flares. When analyzing M class flares, *Sharma et al*. [2004] has shown that the electron temperature will increase by 1.3 to 1.9 times and the ion temperature will increase by a factor of 1.2 to 1.4 times over the normal days average temperature.

The response of the ionosphere to the increased solar flux can be different with each storm. So next it is important to look at the solar irradiance and how variations in it will cause changes in temperatures and densities in the ionosphere.

2.3 Solar Irradiance

The solar irradiance is the total amount of solar energy received at the top of the earth's atmosphere per unit area per unit time (Wm^{-2}). The total solar irradiance varies by 0.1% with the solar cycle, with an average value of 1366 Wm^{-2}. It has been shown by *Hinteregger* [1981], from data that was obtained from a spectrometer on the NASA Atmosphere Explorer (AE-E) satellite, that irradiance values below 180 nm change significantly with solar cycle. Figure 2 shows the ratio of solar maximum to solar minimum irradiance for wavelengths below 180 nm. The variability of these wavelengths is evident in the figure.

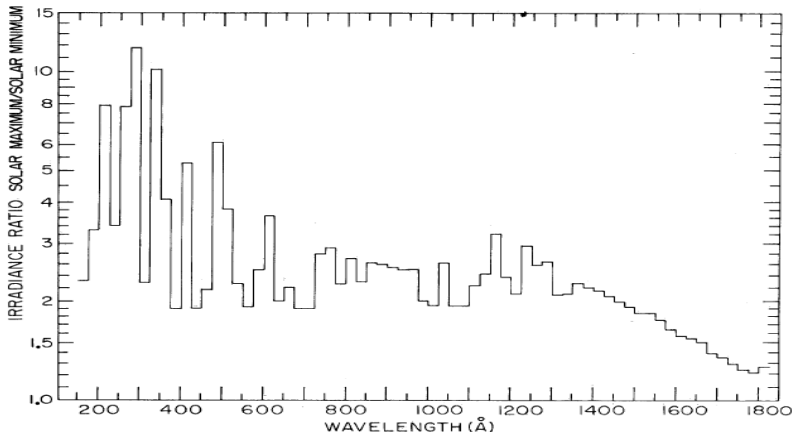

Figure 2. The ratio of solar spectral irradiance near solar maximum, January 1979 to the irradiance near solar minimum, July 1976. Wavelengths bins are in 25 angstrom intervals [*Hinteregger*, 1981].

These shorter wavelengths (< 180 nm) are completely absorbed by the ionosphere. This increase in energy deposition affects the composition of the ionosphere and its properties. The variability of this irradiance is sometimes described by using the sunspot number or the 10.7 cm solar radio flux (F10.7). F10.7 is the radio emission (flux) by the sun at a wavelength of 10.7 cm at the earth's orbit. This is a global daily value measured at local noon at the Pentictin Radio Observatory in Canada.

During a solar flare, only the EUV and x-ray part of the solar spectrum (wavelengths less than 105 nm) will fluxuate significantly. The EUV wavelengths can double in value while the x-ray wavelengths can increase by 100 times the pre-flare irradiance values. This irradiance increase is what drives changes in the ionospheric density, temperature, and heating rates. Researchers have developed proxies to describe the irradiance variations at these shorter wavelengths, which in turn are used in models to drive the changes in the ionosphere during solar flares.

2.4 Electron/Ion Temperatures

The solar irradiance, through ionization and heating, affects the electron/ion temperature and electron density in the ionosphere. So it is important to understand how these parameters change during quiet conditions so that the changes that take place during a flare are better understood.

The electron temperature responds rapidly to changing conditions and is generally in a quasi-steady state. At lower altitudes, the electron temperature is determined by a balance of the heating and cooling processes. This thermal equilibrium prevails at altitudes below 150 to 350 km depending on season, solar cycle, etc. Above this, the

thermal balance is dominated by thermal conduction and can be expressed in the following simplified analytical equation [*Schunk*, Chap 11, 2000],

$$T_e = [T_{eb}^{7/2} - \frac{7}{2}(\frac{q_{et}}{7.7\times10^5})(z - z_b)]^{2/7} \quad (1)$$

where T_{eb} (K) is the electron temperature at the bottom boundary of the thermal conduction regime, q_{et} ($eVcm^{-2}s^{-1}$) is the electron heat flow through the top boundary and z_b (cm) is the altitude of the bottom boundary. This equation shows that if there is a downward heat flow through the top of the boundary ($q_{et} < 0$) then T_e increases with altitude.

Figure 3 shows calculated neutral, ion, and electron temperatures and how they change diurnally. Below the F peak or ~300 km, the electron temperature is controlled by thermal equilibrium and above by thermal conduction. The left panel is during the day when photoelectron heating plays a significant role in increasing the temperature below 280 km. Above this, the temperature is due to a large downward flux of electron heat flow at 800 km. At night (right panel), the heat source is absent and the temperature decreases below 280 km, while above this a downward flux of heat maintains the electron temperature.

The ion temperatures are controlled by collisional coupling to hot thermal electrons and cooler neutrals. At low altitudes, coupling to neutrals dominates and the ion temperature is equal to the neutral temperature both day and night. As the altitude increases, coupling to the hot electrons becomes more important and the ion temperature will increase.

Sharma et al. [2004] has shown that the temperature response of the ionosphere to solar flares is correlated with local time for small flares. Enhancement of electron and ion temperatures is at a maximum at sunrise with progressively smaller enhancements as

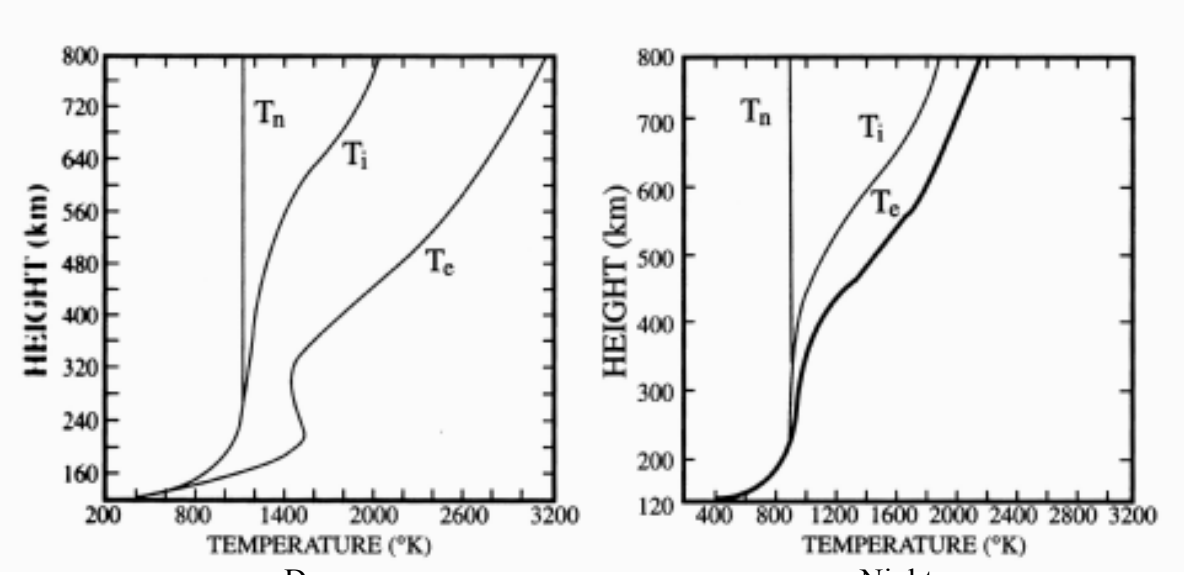

Day Night

Figure 3. The figure shows the calculated electron, ion, and neutral temperature as a function of altitude for the ionosphere. The left diagram is during the day and shows how photoionization will increase the electron temperature (T_e), the ion temperature (T_i), and the neutral temperature (T_n) while at night they decrease. [*Schunk*, Chap 11, 2000].

the day progresses. Electron temperatures can be increased up to 1.9 times the daily average and the ion temperature can be up to 1.4 times the daily average.

Holding all other loss and gain processes constant, the electron temperature is inversely related to the electron density. Figure 4 shows electron temperature and density profiles for the daytime mid-latitude ionosphere for both solar minimum and maximum. This figure is a good example of the inverse relationship between electron temperature

and density. During solar maximum the electron temperature decreases while the electron density increases and vice versa for solar minimum.

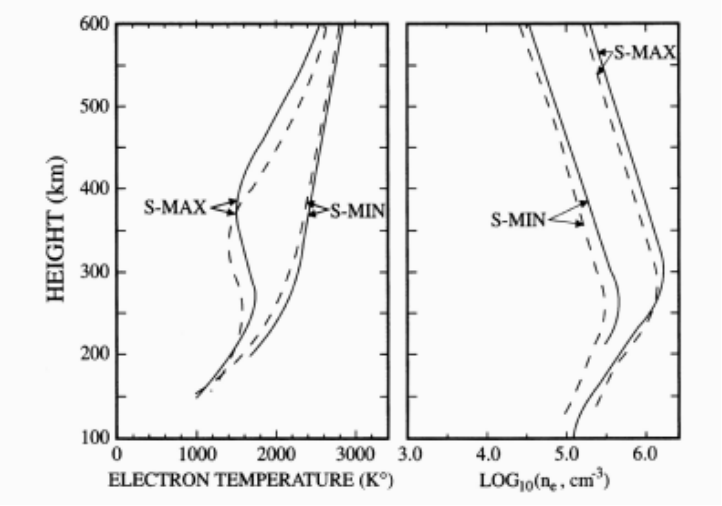

Left Right

Figure 4. Electron temperature and density profiles for the daytime mid-latitude ionosphere at equinox for both solar minimum and maximum conditions. The solid curves are measured profiles while the dashed are calculated, note the inverse relationship between temperature and density [*Schunk*, Chp11, 2000].

2.5 Electron Density

The solar irradiance affects the electron densities differently above and below the F peak. The electron density below the F region peak is controlled by ionization which is under strong solar control. The ionization reaches a peak when the solar zenith angle is at its smallest, around noon. Above the F region peak, some ionization does occur, but diffusion, interhemispheric flow and neutral winds have a greater influence on electron density concentrations. Hence there is less solar zenith angle dependence and peak ionization is reached late in the afternoon.

During a solar flare, the increase in plasma temperature will cause the plasma scale height[4] to increase. This will cause the F_2 region to expand and force diffusion to higher altitudes; changing the overall ionospheric profile.

2.6 Photoelectrons and Electron Heating Rates

Photoelectrons are formed from the excess energy of photoionization. Equation 2 shows this relationship:

$$m + h\nu \rightarrow m^+ + e^- \tag{2}$$

Equation 2 shows that a photon (hν) interacts with a molecule (*m*) and produces an ion (m^+) and a photoelectron (e^-). The conservation of momentum shows that the excess energy of ionization will be imparted to the lighter electron as kinetic energy. Because photoelectrons are a by-product of photoionization, their production is also dependant on the solar irradiance. The photoelectron production rate, $P_e(E,\chi,z)$, is described in Equation 3.

$$P_e(E,\chi,z) = \sum_l \sum_s n_s(z) \int_0^{\lambda_{si}} I_\infty(\lambda) \exp[-\tau(\lambda,\chi,z)] \sigma_s^i(\lambda) p_s(\lambda, E_l) d\lambda \tag{3}$$

Where n_s is the number density, I_∞ is the irradiance at the top of the atmosphere, $\exp[-\tau,\chi,z]$ is the optical depth, σ is the wavelength dependant total ionization cross section, $p_s(\lambda,E_l)$ is the branching ratio for a given final ion state with ionization energy level E_l, and λ_{si} is the ionization threshold wavelength for neutral species s, and ion states *l* [*Schunk*, Chap 9, 2000]. In this equation, I_∞ is the variable that is changed in the model to allow for variations in irradiance due to the solar flare.

[4] The scale height (H) defines the vertical distance over which concentration falls off to about 37% of its original value. H=kT/mg, k-Boltzmann's constant, T-temperature, m-mass, g-gravity

Photoelectrons are important in secondary ionization and in determining the electron heating rate in the ionosphere. Secondary ionization is the result of primary photoelectrons ionizing neutrals which create secondary photoelectrons. It has been shown that secondary ionization increases the total ionization rate by approximately 30% in the F_2 region and by 100% in the E and F_1 regions [*Titheridge,* 1996]. Full calculations are difficult because the upward and downward photoelectron fluxes must be calculated as a function of energy and height. Figure 5, which was computed using an ionospheric model, shows how the ion production rates vary with altitude when including both photoionization rates and total ionization rates[5]. These rates are for summer solar minimum at 1300 L[6]. Note at the peak ionization rates, that O_2^+ changes by only 8% at 104 km with the addition of electron impact ionization rates, while O^+ changes by 28% at 160 km and N_2^+ changes by 24% at 148 km. The greatest increases are seen below 130 km with increases as much as 79% for O^+, 88% for N_2^+ and 11% for O_2.

Most ionospheric models use a fixed correction factor for a given height to account for the effects of photoelectrons, but this fixed value does not allow for any effects from a solar flare. Figure 6 has also been computed by an ionospheric model and it shows photoionization rates that are plotted against total photoionization rates, but this time it is during a flare. Here the peak ionization rates have changed along with the percentage of increase in total ionization. With the addition of the electron impact ionization rates, O_2 changed by 54% at 104 km, O changed by 77% at 116 km and N_2 changed by 87% at 108 km. Electron impact ionization rates are significantly higher

[5] Total ionization rate refers to photoionization rates plus electron impact ionization rates.
[6] 1300 L is the time of peak ionization rate.

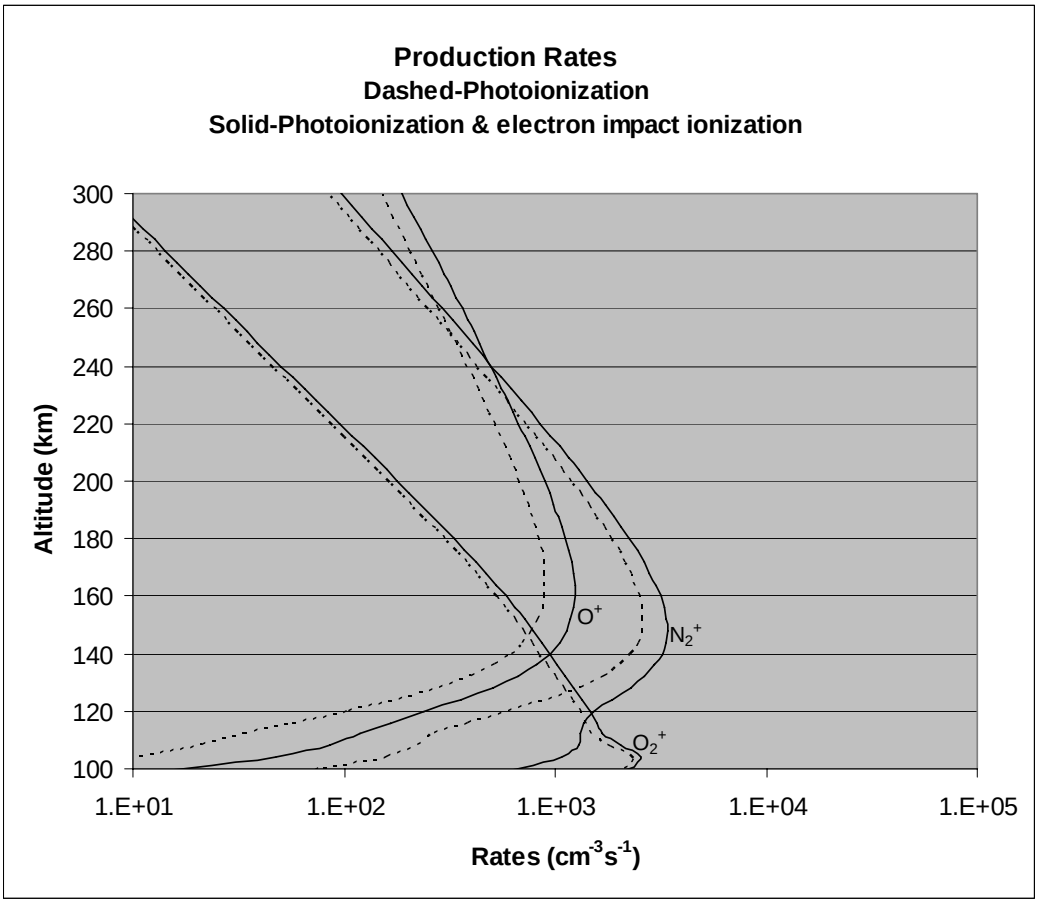

Figure 5. Photoionization rates (dashed lines) compared to total photoionization rates (solid lines) for a non-flare time. Profile is for summer solar minimum, latitude 41.7° at 1300 L.

during flare time than non-flare time, so parameterization of the non-flare time rates will not work if you want to include the effects of a flare in the ionospheric model.

Another way to show this effect of increased ionization rates during a flare is to look at the ratios of electron impact ionization rates to photoelectron ionization rates. Again these rates were calculated using an ionospheric model and are similar in results to that of *Richards et al.* [1988]. Figure 7 shows the ionization ratios for O^+, O_2^+ and N_2^+

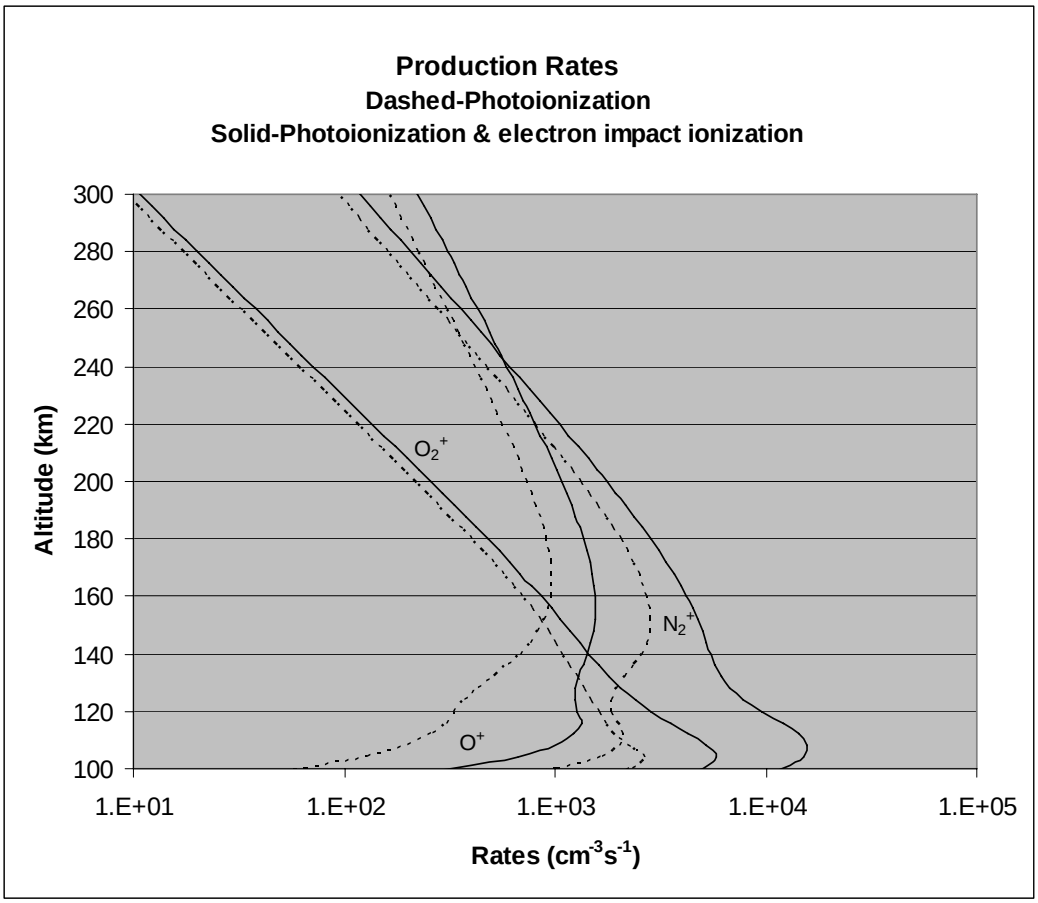

Figure 6. Photoionization rates (dashed lines) compared to total photoionization rates (solid lines) during peak flare. Profile is for summer solar minimum, latitude 41.7° at peak flare time.

for a non-flare time and a flare time. Electron impact ionization becomes much more important during flare time than non-flare time, especially at altitudes below approximately 140 km. The ratio changes by a magnitude of 10 for O_2^+ at 112 km and by a magnitude of ~5 for O^+ and N_2^+ at altitudes above 125 km. The increased ratio at low altitudes is due to the greater attenuation of photons responsible for photoionization.

Photoelectrons are also needed to calculate the electron heating rate. In the ionosphere significant heating of the electrons takes place in the sunlit regions due to

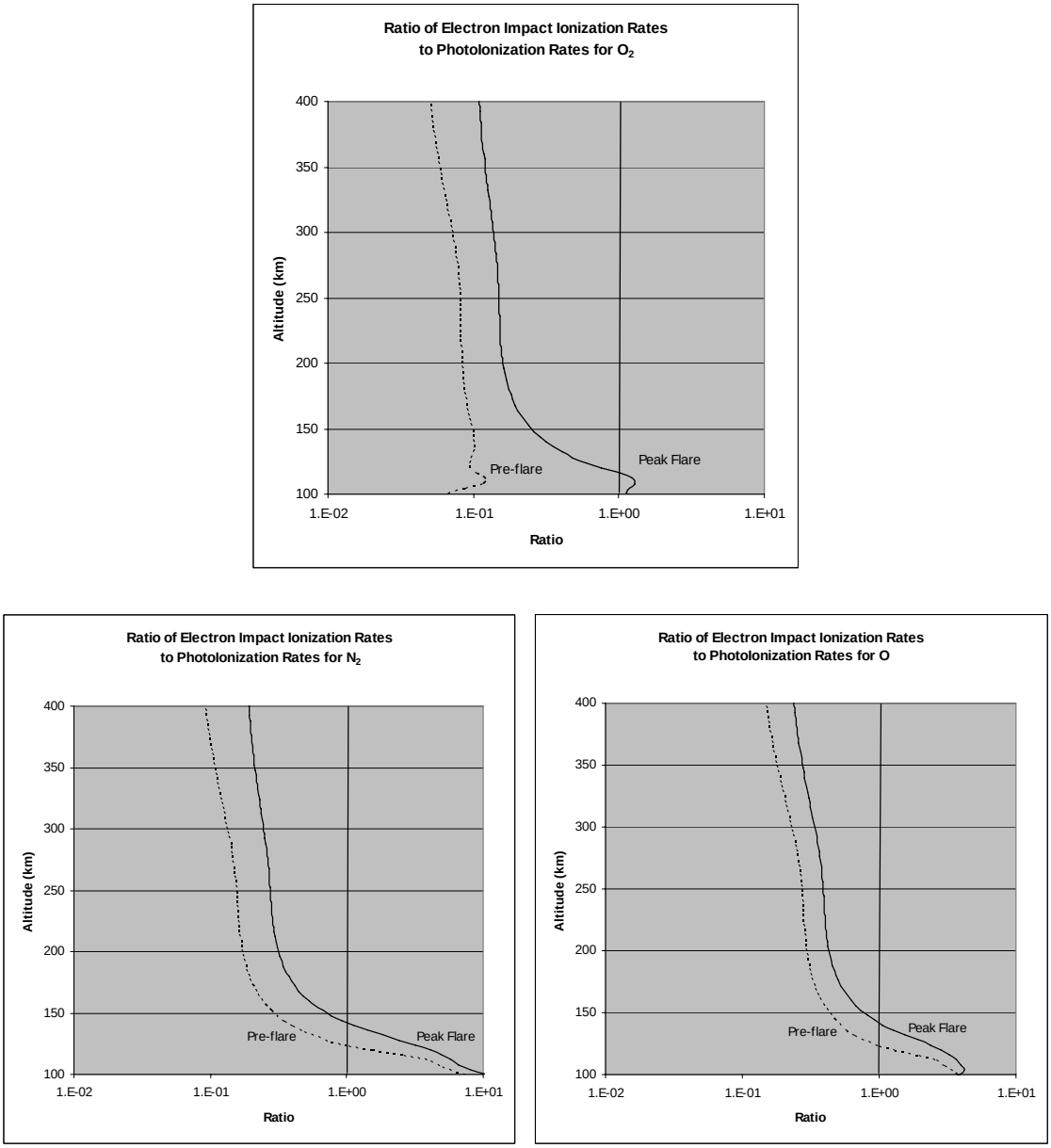

Figure 7. The ratio of electron impact ionization rates to photoionization rates for O_2^+, N_2^+, and O^+ as a function of altitude for a pre-flare (dashed) time and a peak flare time (solid). Profiles are for summer solar minimum at latitude 41.7°.

photoelectrons. Low-energy photoelectrons (≤ 2 eV) directly transfer energy to the thermal electrons by Coulomb collisions. The more energetic photoelectrons can escape

the ionosphere; this energy is then conducted back down to the conjugate ionosphere via magnetic field lines, thus increasing the electron temperatures.

The full electron energy equation is difficult to solve, so *Schunk* [1988] uses a parameterization of the electron volume heating rate based on the F10.7 and the solar zenith angle, but again this will not account for the increase in solar irradiance output caused by solar flares.

2.7 Understanding Ionograms

Ionograms represent the electron density structure of the ionosphere. This is accomplished by using radio soundings of different frequencies. These soundings show the variation of the virtual height of a reflection as a function of the radio frequency. The virtual height is the reflection height calculated assuming the waves travel at the speed of light, but in the ionospheric plasma the waves travel at less than the speed of light; because of this the virtual height is greater than the actual height of reflection. Figure 8 is showing a simple schematic of this relationship.

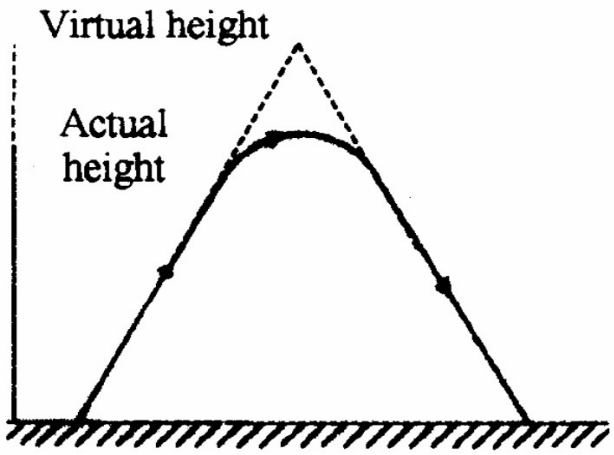

Figure 8. Relationship between the virtual and actual height for vertical and oblique propagation.

Generally two wave modes are reflected back, one is the ordinary wave (o) the other the extraordinary wave (x). These correspond to the different propagation modes of the wave in the presence of a magnetic field. For clarity, reference will be made only to the ordinary mode in this research; although in practice both are used to describe the ionosphere.

Ionograms are affected by three parameters, the electron density (N), the total magnetic induction (B) and the angle between the magnetic field and the direction of propagation. In this research the electron density is the parameter of interest. The relationship between N and electron plasma frequency f, for vertical propagation is shown in Equation 4.

$$f\,(kHz) = 9\sqrt{N_e\,(cm^{-3})} \tag{4}$$

In passing through the ionosphere, the electron density (N) increases with altitude until the F_2 peak, when it starts to decrease with altitude, this occurs at approximately 300 km. The highest frequency that can be reflected from a given ionospheric region is called the critical frequency (f) which is indicated by asymptotes or cusps in the virtual height. Figure 9 shows a typical ionogram with the critical frequencies and virtual height of the different regions of the ionosphere annotated. These different regions correspond to the regions in the density profile of Figure 10. This figure plots the electron density as a function of actual height. The frequency peaks can be seen to be at lower altitudes here than the virtual heights plotted on the ionogram in Figure 9. The densities above the f_oF_2 peak[7] in Figure 10 must be obtained via satellite measurements or other techniques.

[7] In f_oF_2, the o indicates that this is from the ordinary trace.

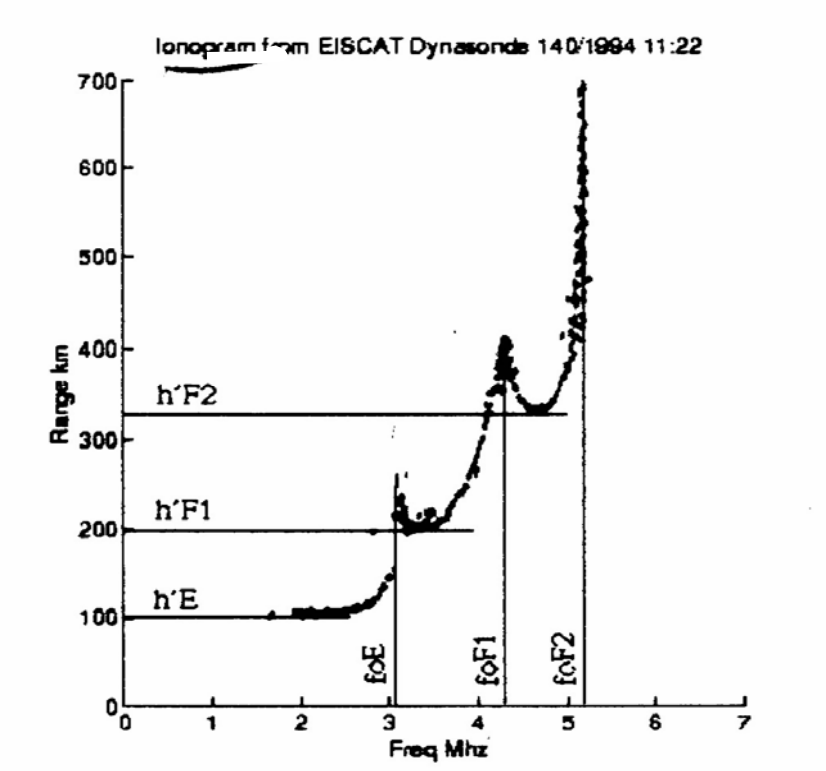

Figure 9. This figure shows a vertical electron density profile, or ionogram, which is measured by sweeping through a range of frequencies.

2.7.1 Bear Lake Dynasonde

The Bear Lake dynasonde is located at Bear Lake Observatory near Utah State University. The dynasonde produces ionograms at 5-minute intervals which can be combined into a 12-hour plot showing how the ionosphere changes over time. These ionograms are ideal in showing the ionospheric changes in response to solar flares as long as the flares are not so large that D-region absorption[8] blocks the entire signal. This

[8] D-region absorption occurs when no signal is returned to the dynasonde due to increased electron densities in the D-region.

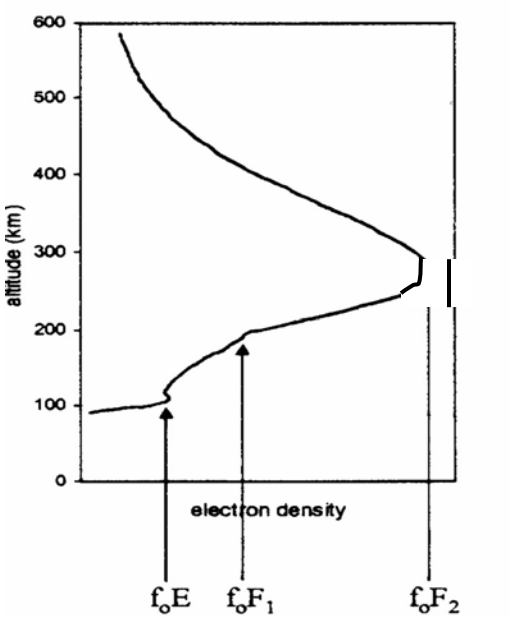

Figure 10. This is a plot of the electron density in the ionosphere versus actual height. The frequency peaks from the ionogram of Figure 9 corresponds to the peak electron density at each layer.

limits the flares studied to X1 class or lower. These plots will be used to compare to the modeled ionograms in this research.

Figure 11 is an example of a 12-hour ionogram from NGDC for 11 May 2004. The flare starts at 19:23 UT, peaks at 19:37 UT and is over by 19:54 UT. This was a class M1.1 flare. Note the D-region absorption during the flare is indicated by the white intrusion in the lower frequencies during flare time. There is also a frequency decrease during flare time at f_oF_2 that *Smithtro et al* [2004] termed a flare notch. The flare notch is believed to be due to enhanced electron temperatures due to heating by photoelectrons. As the temperature increases, the electron density will correspondingly decrease due to F region expansion and diffusion. This is most often seen during an M-class flare that

occurs near local noon. The other notching that appears in the f_oF_2 boundary is possibly due to traveling ionospheric disturbances[9]. Local maxima in the E and F_1 regions, which produce asymptotes or cusps in the standard ionogram, appear as inversions of the virtual height in a 12-hour plot, these areas are indicated in the diagram as f_oE and f_oF_1.

2.8 Previous Work

There has been much work done regarding solar flares and their effects on the ionosphere. Researchers have looked at how large flares can increase the total electron content (TEC) by 5-7 TEC unit[10] [*Hubba et al.*, 2005; *Tsurutani et al.*, 2005]. They have studied the increased electron and ion temperatures due to moderate flares and have shown that the temperature increase is dependent on the time of day the flare takes place [*Sharma et al.*, 2004]. *Huba et al.* [2005] have shown that for large flares, the maximum electron density in the F-layer will increase by 20%, and that the altitude of this maximum will decrease by 20%. The solar spectral irradiance has been studied by *Meier et al.* [2002] who has shown that for large flares the x-ray radiation can increase by more than a factor of 200 and that the EUV enhancement increases by much less, only about 50%. And finally the photoelectron response to a large flare has been studied by *Woods et al.* [2003]. They have shown that high energy electrons increase by a factor of 10 while low-energy electrons change very little.

The current effort is built upon the previous work done by *Smithtro et al*. [2004], which examined moderate solar flares using an ionospheric model. They found enhancements in the E and F_1 regions while the electron density in the F_2 region

[9] Traveling ionospheric disturbances are waves in the F region of the ionosphere that propagate equatorward from high latitudes. They have intermittent regions of decreased electron density.
[10] 1 TEC unit = 10^{16} m^{-2}

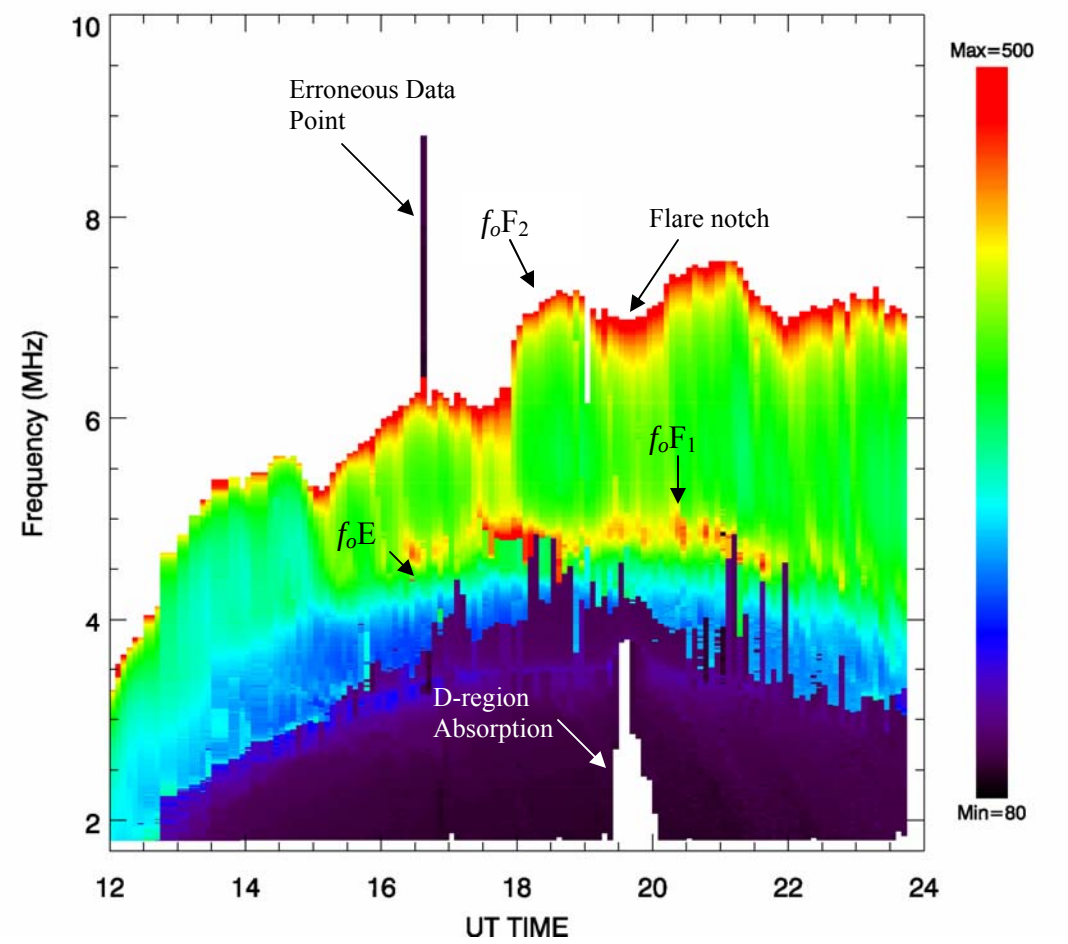

Figure 11. A 12-hour ionogram plotted with data from NGDC for 11 May 04.

simultaneously decreased with moderate solar activity. They were able to model this outcome using a modified ionospheric model, and found that the decrease is due to enhanced temperatures which change the scale height moving the plasma to higher altitudes. Figure 12 shows a measured ionogram from Bear Lake Observatory compared to a modeled ionogram from the *Smithtro et al.* [2004] model.

These ionograms indicate where the E and F_1 region increase in electron density is located and the F_2 region electron density decrease is also shown. The differences seen

in Figure 12 between the real and modeled ionograms may be due to the simple model applied for flare response and the irradiance or the simplistic treatment of secondary ionization by photoelectrons [*Smithtro et al*., 2004].

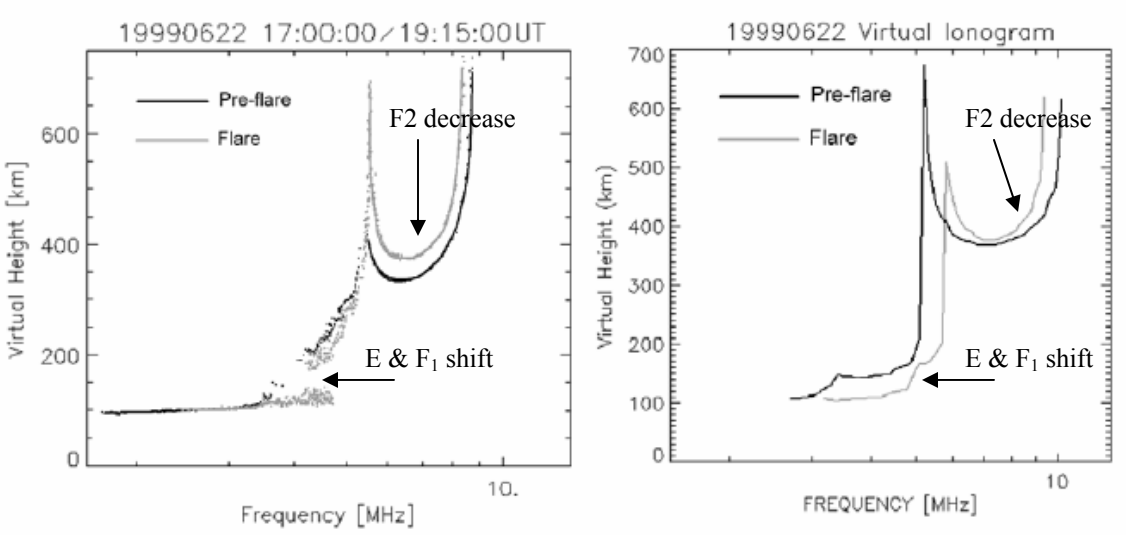

Figure 12. A comparison between a measured ionogram and a modeled ionogram using an ionospheric model modified by *Smithtro et al*. [2004] to include the effects of flares.

2.9 The Models

In this section the background on the three primary models are given. Discussed first is the main ionospheric model; the Time-Dependent Ionospheric Model (TDIM) which develops the ionospheric profiles used in this research. This will be followed by a discussion on the models that will be integrated into the TDIM; the Flare Irradiance Spectral Model (FISM) and the Glow model.

2.9.1 The Time-Dependent Ionospheric Model

The TDIM is a comprehensive, multi-ion (NO^+, O_2^+, N_2^+, O^+, N^+, He^+) model of the middle and high latitude ionosphere. It solves the continuity (5), momentum (6), and energy (7) equations as a function of height for an inclined magnetic field at E and F region altitudes (100 to 800 km).

$$\frac{\partial n_s}{\partial t} + \nabla \cdot (n_s \vec{u}_s) = P'_s - L'_s n_s \tag{5}$$

$$n_s m_s (\frac{D_s \vec{u}_s}{Dt}) + \nabla p_s + \nabla \cdot \vec{\tau}_s - n_s m_s \vec{G} - n_s e_s [\vec{E} + u_s \times \vec{B}] = \frac{\delta \vec{M}_s}{\delta t} \tag{6}$$

$$(\frac{D_s}{Dt})(\frac{3p_s}{2}) + (\frac{5p_s}{2})(\nabla \cdot \vec{u}_s) + \nabla \cdot \vec{q}_s + \vec{\tau}_s : \nabla \vec{u}_s = \frac{\delta \vec{E}_s}{\delta t} + Q_s - L_s \tag{7}$$

Where $D/Dt = \delta/\delta t + \vec{u}_s \cdot \nabla$ is the convective derivative of species s, $p_s = n_s k T_s$ is the partial pressure, n_s is the number density, m_s is the mass, e_s is the charge, T_s is the temperature, $\mathbf{u}_s$ is the drift velocity, $\mathbf{q}_s$ is the heat flow vector, τ_s is the stress tensor, P'_s is the ionization production rate, L'_s is the ionization loss frequency, Q_s is the heating rate, L_s is the cooling rate, G is the acceleration due to gravity, E is the electric field, B is the magnetic field, $\delta/\delta t$ is the time derivative, ∇ is the coordinate-space gradient, and k is Boltzmann's constant. $\delta \vec{M}_s / \delta t$ and $\delta \vec{E}_E / \delta t$ represent the rate of momentum and energy exchange in collisions between species s and the other species in the plasma [*Schunk*, 1988]. In these equations, the production and loss terms will be modified to include more rigorous calculations of the electron impact ionization rates and the electron heating rates.

The three-dimensional structure of the ionosphere is obtained by following a co-rotating plasma flux tube as it convects through the neutral atmosphere. This model takes into account diurnal variations, convection electric fields and particle precipitation. The ion and electron energy equations are also solved [*Schunk*, 1988]. The neutral gas specifications are computed using the Mass Spectrometer Incoherent Scatter empirical model (MSIS-86) [*Hedin*, 1991].

Although the TDIM models the ionosphere accurately during solar quiet days, there are two shortfalls to this model if one wants to see how the ionosphere changes in time due to solar flares. First, the irradiance used is from the Extreme UltraViolet for Aeronomic Calculations (EUVAC) model [*Richards et al*., 1994] which relies on the F10.7 proxy that is measured only once per day. Because of this, the TDIM has no inherent capability to specify the irradiance changes during a solar flare. Second, the model does not include the effects of photoelectrons, which in turn are responsible for secondary ionization and electron heating. These shortfalls must be corrected to accurately reflect the effects of a solar flare on the ionosphere.

In the modified TDIM, *Smithtro et al*. [2004] accounted for these issues by creating a flare-time irradiance model, using a parameterized fit to the results of *Woods et al*. [1998]. They were able to use irradiance measurements made by the SEE on the TIMED satellite to develop a ratio of flare irradiance to pre-flare irradiance [*Woods et al*., 1998]. The SEE instrument, as stated earlier, was designed to measure the spectral irradiance between 0.1 and 195.0 nm for approximately one 3-minute interval per 97 minute orbit. This would normally make the data unsuitable for solar flare studies, but fortuitously on 21 April 2002, the TIMED satellite measured an X1 flare prior to onset

and just after its peak. Using this data, *Woods et al.* [1998] developed a ratio of flare irradiance to pre-flare irradiance to approximate the irradiance increase during a moderate x-ray flare event.

Figure 13 illustrates the energy flux ratio which was used to create a flare-time irradiance model as an addition to the EUVAC model. In order to develop the model over time, the GOES soft x-ray flux is used as a proxy. This data is fit using a lognormal function, which provides an analytic expression to compute a scale factor as a function of time. This scale factor is used to develop the behavior of the flare over time and is then applied to the EUVAC irradiance [*Smithtro et al*, 2004]. The current work will improve upon this approach by using irradiances derived from the FISM model, which will be discussed in the next section.

The second shortfall of the TDIM model is that it does not self-consistently include the effect of photoelectrons. Photoelectrons cause secondary ionization when they collide with the neutral gas and they also heat the ambient thermal electrons via coulomb collisions. The wavelengths below 31 nm are important for calculating the photoelectron flux. *Richards and Torr* [1988] showed that the longer wavelengths are attenuated more efficiently than the shorter wavelengths, so that photoelectron impact ionization becomes most important at lower altitudes. Recall Figure 7, which depicts the ratios of electron impact ionization rates to photoionization rates. The attenuation effect from the increased energy at shorter wavelengths is clearly seen in these plots. TDIM approximates this additional ionization by applying a simple altitude and species dependent scale factor to the photoionization rate [*Richards and Torr*, 1988].

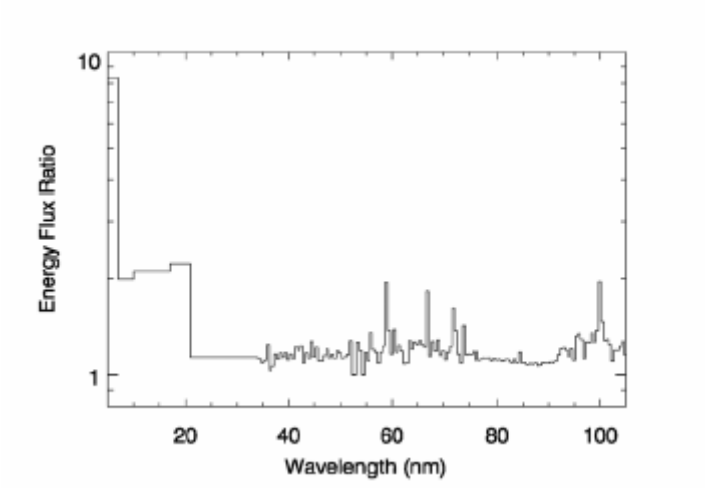

Figure 13. The ratio of the flare irradiance to the pre-flare irradiance is shown as a function of wavelength. The measurements were made by the SEE instrument on the TIMED satellite at 0026 and 0233 UT [adapted from *Woods et al*., 2003].

During a solar flare the additional photon flux in the shorter wavelengths increases the photoionization rates below 150 km. Depending on the intensity of the flare, the rates can increase by as much as 100%. This effect will be seen in the results of this research.

The electron heating rate used by *Schunk* [1988] is based on a model from *Richards and Torr* [1984] and it computes the solar EUV heating rate by using a parameterization of the electron volume heating rate based on F10.7 and the solar zenith angle (see Figure 14). This process does not allow for changes during a solar flare. *Smithtro et al*. [2004] introduced a simple flare-time increase to the volume heating rate. This was done by calculating the ratio of solar maximum to minimum heating rates, and then applying an altitude dependent correction as a scale factor to represent the changes induced by the X1 flare discussed above. A lognormal fit to the GOES satellite x-ray

flux data was used as a proxy to drive changes in the volume heating rate over the course of the flare [*Smithtro et al*, 2004]. In the current work, this heating rate will be replaced by more rigorously calculated values from the Glow model.

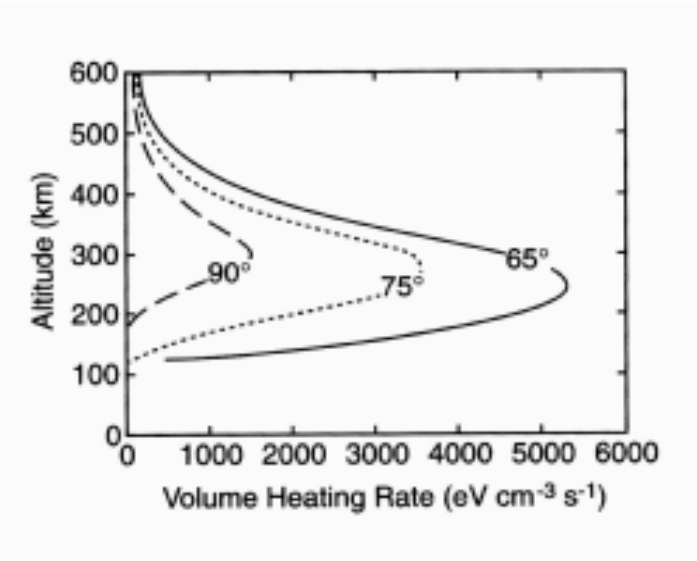

Figure 14. The electron heating rate as a function of altitude for solar EUV sources. The EUV heating rate is shown for several solar zenith angles and was calculated using the method described by *Richards and Torr* [1984] [*Schunk*, 1988].

2.9.2 The Flare Irradiance Spectral Model

Chamberlain [2005] created FISM as an empirical model that uses proxies to determine the solar XUV, EUV, and FUV irradiances (0.1-195 nm) at a 1-nm spectral resolution in one minute time intervals. Daily proxies that are formed in the same layer of the solar atmosphere as the wavelengths that are being modeled, such as Mg II core-to-wing ratio and Lyman alpha, are used to model the 11-year solar cycle and 27-day rotational period irradiance variations of the sun. These proxies are from the data measured by the Solar EUV Experiment (SEE) onboard the Thermosphere, Ionosphere,

Mesosphere, Energetics and Dynamics (TIMED) satellite. The SEE instrument measure the full-disk solar vacuum ultraviolet (VUV) irradiance from 0.1 to 194.5 nm. The irradiance is measured in 1 nm intervals for 3-minutes every orbit (97 minutes), which gives 14-15 observations per day. SEE has been collecting data since 2002 and is considered to have the most accurate irradiance measurements to date. In order to model irradiance changes in intervals less than a day, the 3-second flux values from the GOES 0.1-0.8 nm channel and the positive time derivative of this flux was used.

Compared to the EUVAC, this model improves significantly the irradiance values in the EUV range and also adds algorithms to empirically model flares. Figure 15 shows the standard deviation between the FISM and EUVAC model at minimum and maximum solar conditions. This data uses the daily average for EUVAC for a 54-day period and is in 5 nm bins. There are large differences between the models, but FISM data has been shown by *Chamberlain* [2005] to agree with the data from the TIMED SEE to within 10%. The TIMED SEE data are the most accurate EUV measurements available. Since FISM is accurate to within 10% of the TIMED SEE data, Figure 15 shows the large discrepancies between the measured data and the EUVAC model.

The wavelengths below 105 nm have the greatest impact on ionization in the lower ionosphere, affecting the electron/ion densities and temperatures in the E and F_1 regions of the ionosphere. It is also these wavelengths that undergo the greatest variation during solar flares. Depending on the size of the flare, increases can be more than 10 times the normal irradiance values, causing large variations in the lower ionosphere. These are variations that EUVAC cannot model during a solar flare.

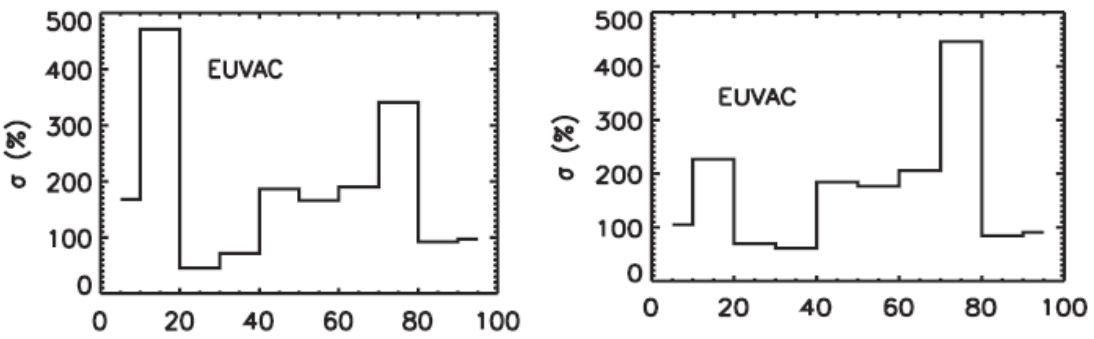

a. b.

Figure 15. The standard deviation between measured data and EUVAC at (a.) minimum and (b.) maximum solar conditions for a 54-day period separated in 5 nm bins [*Chamberlain*, 2005].

2.9.3 The Glow Model

The Glow model, developed by *Solomon*, [2005], uses an input solar spectrum to calculate photoelectron ionization, auroral electron ionization (not used in this research), and electron heating rates. Photoelectron transport, including cascade and secondary ionization processes, is computed using the two-stream method by *Nagy and Banks*, [1970]. The two-stream method performs calculations in the upward and downward directions and since electrons follow magnetic field lines, this is a good approximation. In the Glow model, the neutral atmosphere is assumed to vary with altitude. Electrons follow a slant path from the top of the atmosphere to the base (100 km). The electrons can be scattered forward or backward by elastic collisions or they can be ionized, dissociated, or excited through inelastic collisions [*Bailey et al*., 2002]. Glow calculates all these processes. A model atmosphere for Glow is obtained from the previously mentioned MSIS model and the International Reference Ionosphere-90 (IRI-90). The

MSIS model describes the neutral atmosphere while IRI -90 is used to initialize the electron/ion temperatures and O^+, O_2^+, NO^+ and electron densities.

III. Methodology

The methodology of integrating the models is described in the following sections. Starting with the FISM model and then the Glow model, the results of the integration is looked at for non-flare days and compared to other models and actual data to ensure the integration is developed appropriately.

3.1 Integrating the Models

The FISM model does not have a direct interface with the TDIM model. The model was recently developed by *Chamberlain* [2005] at the University of Colorado and he has yet to develop an interface for the user. Until one is developed, he runs the model for the requested days and sends the data to the user.

The FISM files have 170 wavelength bins from 0.5 to 170 nm, at a one minute cadence. It was made compatible to Glow by readjusting the number of bins to 123 and the wavelength range from 0.5 to 105 nm. The Glow bins vary in wavelength width, smaller widths from 0.5 to 10 nm to capture the large irradiance changes and larger widths at 95 to 105 nm where the change in irradiance is much less. Adjusting the bins was accomplished using an algorithm that combined or divided the irradiance as necessary to get into the appropriate format.

An example of how the ionospheric profile changes with the use of FISM irradiances versus EUVAC is shown in Figure 16. The electron densities along the most of the FISM profile have decreased slightly in comparison to the EUVAC profile. This is due to the irradiance being greater when using FISM causing the electron density to decrease. In Figure 16 the electron temperatures remains the same from 280 to 400 km

and from 220 to 280 km it decreases slightly. This slight decrease doesn't change the electron density but in the area where it stays the same there is a slight increase in electron density.

The increased temperatures in Figure 17 are due to the increased irradiance values of the FISM model. Figure 18 is a plot of the irradiance versus wavelength values for the EUVAC model. These values underestimate the irradiance for this particular day as compared to the FISM irradiance in Figure 19. Figure 19 shows the irradiance values for the FISM model on 12 May 05 at 1200L. These values are greater than EUVAC and cause the electron temperature to increase.

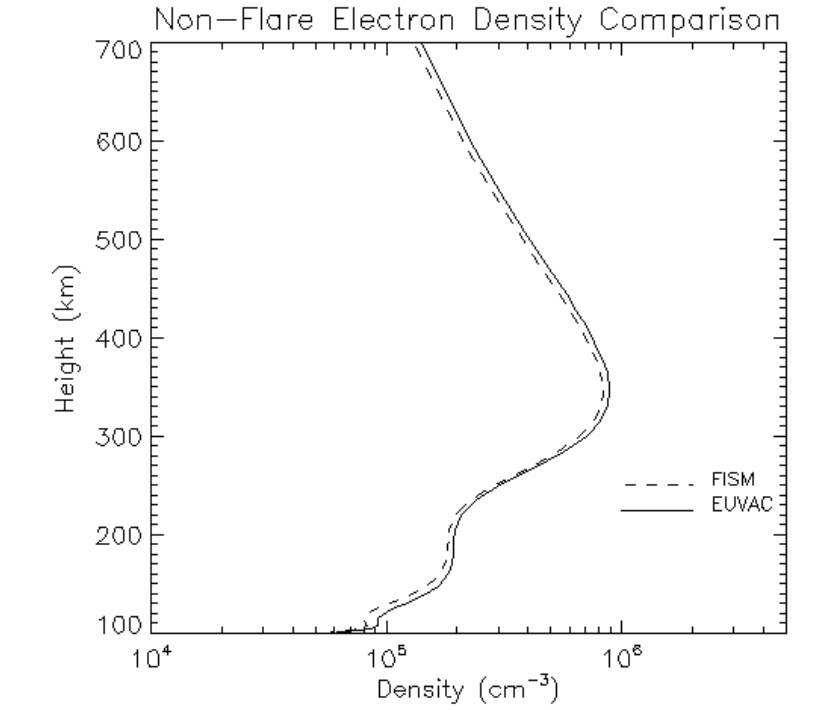

Figure 16. Ionospheric profiles showing electron densities as a function of altitude on a non-flare day; 12 May 05 at 1200L. The solid lines show TDIM using the Glow model with EUVAC irradiance and the dashed lines show TDIM with the Glow model using FISM irradiances.

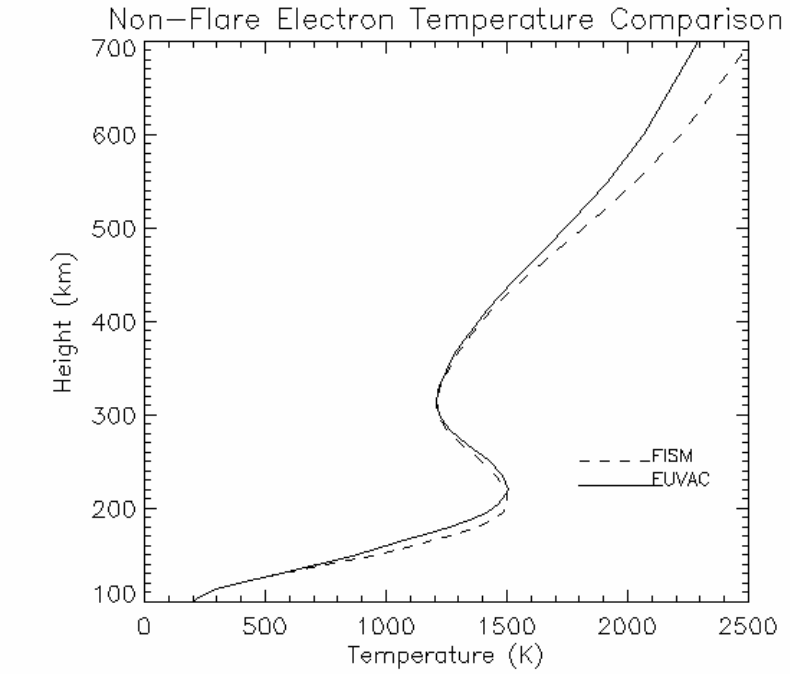

Figure 17. The electron temperature as a function of height. It compares the original TDIM model to the integrated model at 1300 L for a non-flare day. This model was run with the TDIM electron heating rates.

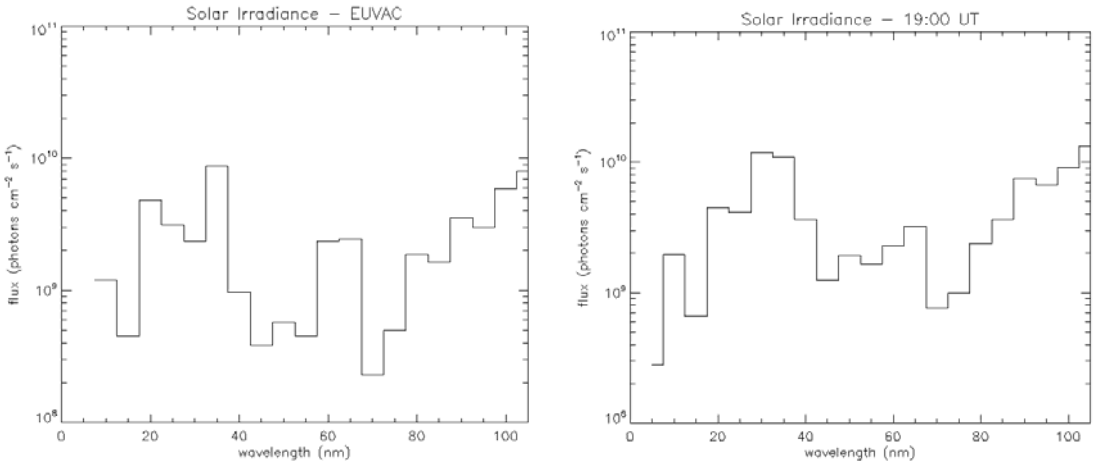

Left Right

Figure 18. The irradiance (flux) is plotted as a function of wavelength using the standard EUVAC irradiance (left) and FISM (right) used in the TDIM model.

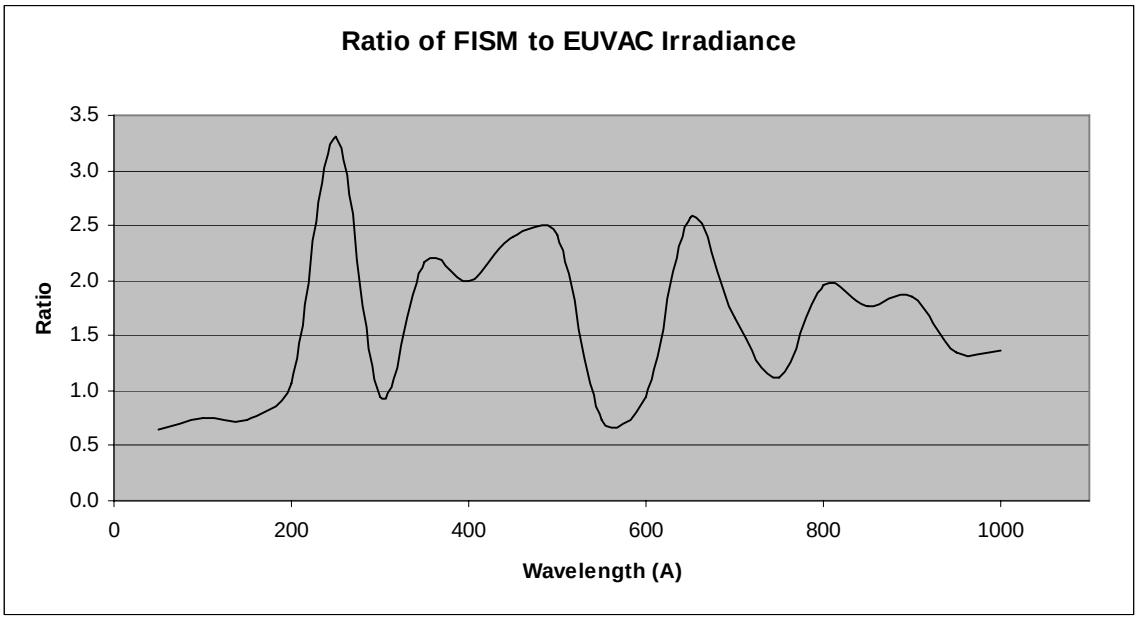

Figure 19. Ratio of FISM to EUVAC irradiance for non-flare time.

The Glow integration was more complicated than the FISM integration. The Glow model outputs that are used for the TDIM are the electron heating rates and O^+, O_2^+, and N_2^+ total ionization rates as a function of altitude. The total ionization rates comprise the photoionization rates plus the electron impact ionization rates.

First the IRI-90 ionosphere temperatures and densities were replaced with the TDIM values. Glow was then run to ensure there were no inconsistencies with these changes; no changes in the output of the TDIM program were noted. Then the photoionization rates in the TDIM were substituted with the rates from Glow, again this was validated to be correct because the densities did not change with the original model. Then the electron impact ionization rates were added to the photoionization rates. The expected changes were seen below 130 km where there was an increase in total ionization rates. Figure 20 shows how important the additional electron impact ionization is below

130 km. It is showing the ratio of electron impact ionization rates to photoionization rates as a function of altitude. The rates are greater than one for O^+ and N_2^+ and there is a slight increase for O_2^+ as well. When Figure 20 is compared to the results of *Titheridge* [1996], the ratio and structure of the profiles are very similar for O^+ and N_2^+. Below 150 km the profile for O_2^+ varies a bit but the ratio is approximately the same. The final change was substituting the Glow heating rates into the TDIM.

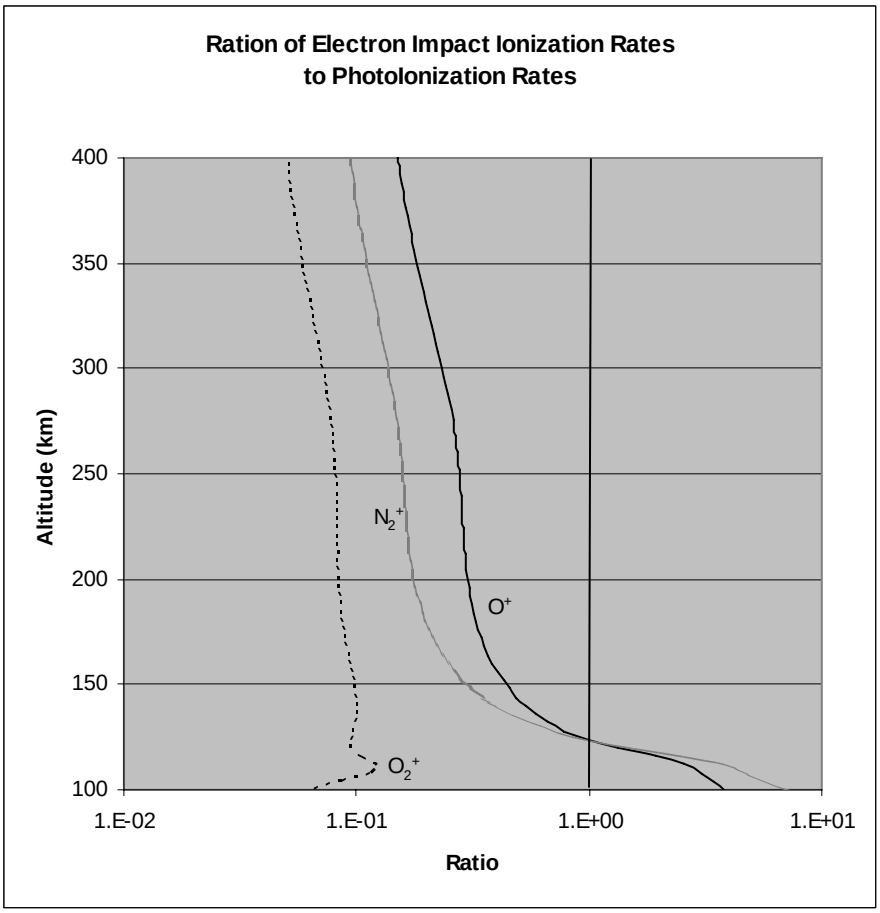

Figure 20. The ratio of electron impact ionization rates to photoionization rates. Data is from early summer solar minimum at 41° latitude, 1300L time, and a solar zenith angle of 25°; this is a non-flare time.

The Glow heating rates made the most dramatic changes to the profiles. The Glow heating rates increased below 130 km and ~25 km above and below the electron heating peak for several profiles that were modeled. Some heating rate profiles increased between 25 and 50% from 100 to 500 km, with a very slight increase to 800 km while other profiles maintained the increase around the electron heating peak but showed a varied increase or decrease beyond 200 km. Figure 21 shows this varied change in heating rates. These changes are due to the FISM irradiance being slightly different

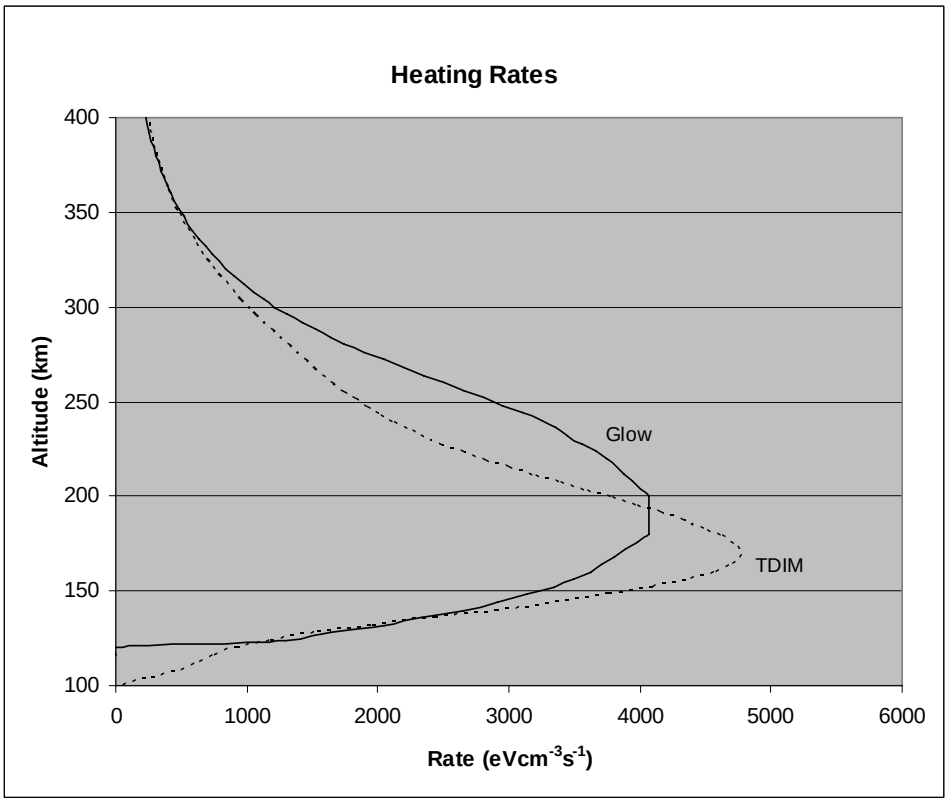

Figure 21. The electron heating rate comparison between TDIM and Glow. Data is from early summer solar minimum at 41° latitude, 1300L time, and a solar zenith angle of 25°; this is a non-flare time.

between the days. There were also changes in the electron density and the electron temperature profiles from substituting in the Glow heating rates.

Figure 22 shows the electron density plotted as a function of altitude. This profile is for a non-flare day at 1300 L. The largest increase in electron density was below 130 km while there was a decrease in the densities from 130 to 230 km. Above 230 km, the electron densities showed a very slight increase. The changes below 230 km were due to decreased calculated photoionization rates by the Glow model. Figure 23 shows the electron temperature plotted as a function of altitude for the same day. The electron temperature increases from ~130 to ~220 km while the electron densities decrease over this altitude range. The electron temperature slowly starts to increase above 400 km with

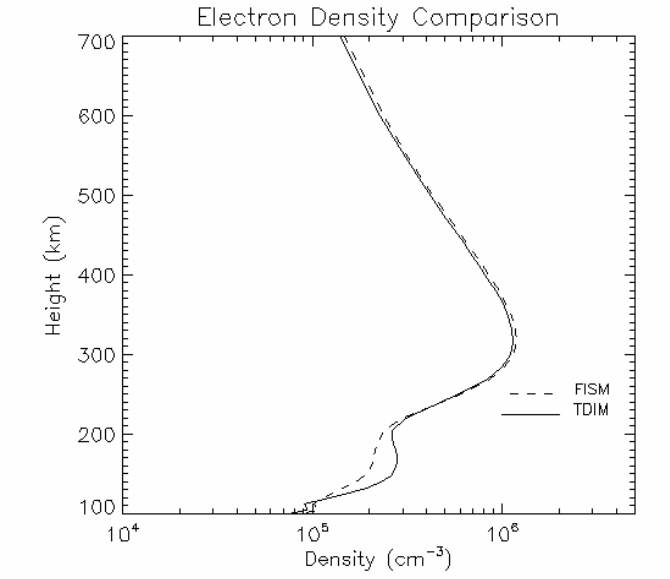

Figure 22. Electron density profile comparison between the original TDIM model and the TDIM modeled integrated with the Glow and FISM models. Data is from summer solar minimum at 41.7° latitude, 1300L and a solar zenith angle of 30.2°; this is a non-flare time.

a maximum change of 400 K at 800 km while the electron density increases just slightly. The increased electron temperatures are due to the increased heating rates in the lower altitudes.

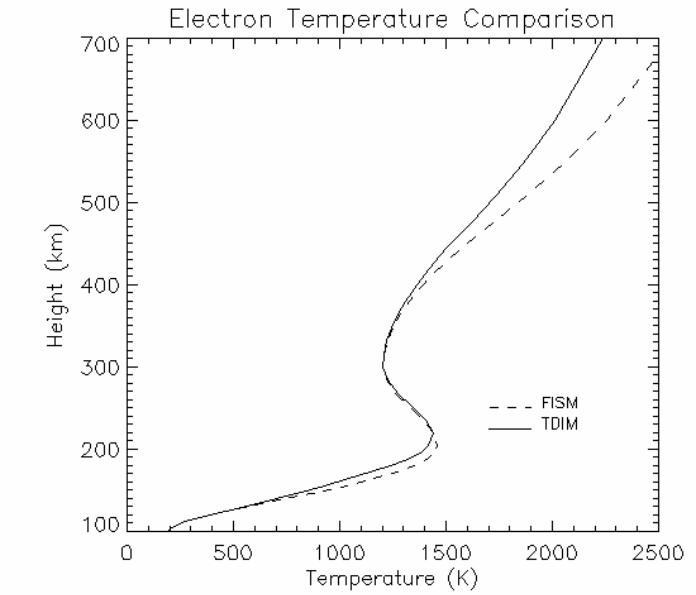

Figure 23. Electron temperature comparison between the original TDIM and TDIM integrated with the Glow and FISM models. Data is from early summer solar minimum at 41° latitude, 1300L time, and a solar zenith angle of 30.2°; this is a non-flare time.

3.2 Comparison to Bear Lake Observatory Ionograms

The Bear Lake ionograms are downloaded from the National Geographic Data Center (NGDC) website and put through an algorithm to get a 12 or 24-hour ionogram. Because of the time involved in downloading this data[11] only 12 hours of this data has been retrieved for each flare. Since this research is only concerned with the flare event and not the entire day's profile, this is a sufficient amount of data to compare to model

[11] 144 files at 3 minutes each = 7.2 hours of downloading

results. This graph is then compared to the modeled output from the combined TDIM, FISM, and Glow model (or the integrated model). The integrated model is run for a 36 hour period to allow for the conditions to equilibrate. Then the last 12 hours from the output is put through an algorithm and plotted. Figure 24 in the next chapter will show an example of this type of ionogram composite. The details of this figure are explained more fully there.

IV. Results and Discussion

4.1 Introduction

Two flares were chosen so that the best noise free data could be retrieved from Bear Lake Observatory. The flares are categorized as a M2.0 and a M1.1 x-ray flare. They occurred around noon local time, so a flare notch should be easily recognizable in the NGDC data. The flares are similar in energy output but the duration of the M2.0 flare was 63 minutes and the M1.1 lasted 31 minutes. The solar zenith angles at the time of the flares peak are 37.6 degrees for the M2.0 and 24.1 degrees for the M1.1 flare.

The following sections will include the measured data downloaded from NGDC to be used as a comparison for the modeled data. The NGDC data will be plotted in a 12-hour ionogram and also as two individual ionograms for pre-flare and peak flare. These will be discussed so that they can be used to compare with the modeled ionograms, which will follow. Then we will look at how diurnal effects will change the different ionospheric density and temperature profiles from pre-flare to peak flare. This will be used as a baseline to compare to the integrated model's profiles. Finally a look at the spectra from the FISM model during pre-flare and peak flare times to see how it affects the outcome of the model.

4.2 M2.0 Flare 4 April 2003

This flare began over Bear Lake Observatory at 19:35 UT (12:35 L), peaked at 20:18 UT (13:18 L) and ended at 20:38 UT (13:38 L). Figure 24 shows a 12-hour ionogram from Bear Lake Observatory, the vertical lines are where the data was missing at 10 and 40 minutes after every hour. Otherwise the data is at a 5-minute cadence.

Figure 25 shows pre-flare and peak flare ionograms from Bear Lake Observatory. These will be used for comparison to the model runs but first an explanation of these figures.

4.2.1 Bear Lake Observatory Ionograms

The 12-hour ionogram in Figure 24 shows a diurnal increase in electron density starting at 1300 UT as indicated by the increase in frequency. The E and F_1 layers start to decrease in electron density at 2100 UT because the solar angle starts to increase, but the F_2 layer continues to increase until 2400 UT. The F_2 layer increase may be due to diffusion or gravity waves since this layers electron density is controlled by processes other than photoionization. The M2.0 flare that began at 19:35 UT is immediately recognizable by the inverted v-notch that is due to D-region absorption during the flare. There is also a small f_oF_2 decrease or flare notch identifiable above the inverted v-notch. The other areas of notching in the f_oF_2 region are possibly due to traveling ionospheric disturbances. The two arrows at the bottom of the figure indicate the approximate times of the ionograms in Figure 25.

The ionograms in Figure 25 were taken at 19:30 UT (black) and 20:20 UT (green). They are plotted as a function of virtual height and frequency. The black cusps in this figure indicate h'E at ~100 km, h'F_1 at ~210 km and h'F_2 at ~275 km. At the peak of the flare h'F_2 and the electron density in the F_2 region decrease slightly during flare time, indicating that the scale height has changed due to the increased electron temperatures.

4.2.2 Integrated Model Ionograms

In Figure 26, the 12-hour modeled ionogram is plotted for comparison to the actual NGDC 12-hour ionogram of Figure 24. The modeled ionogram composite shows

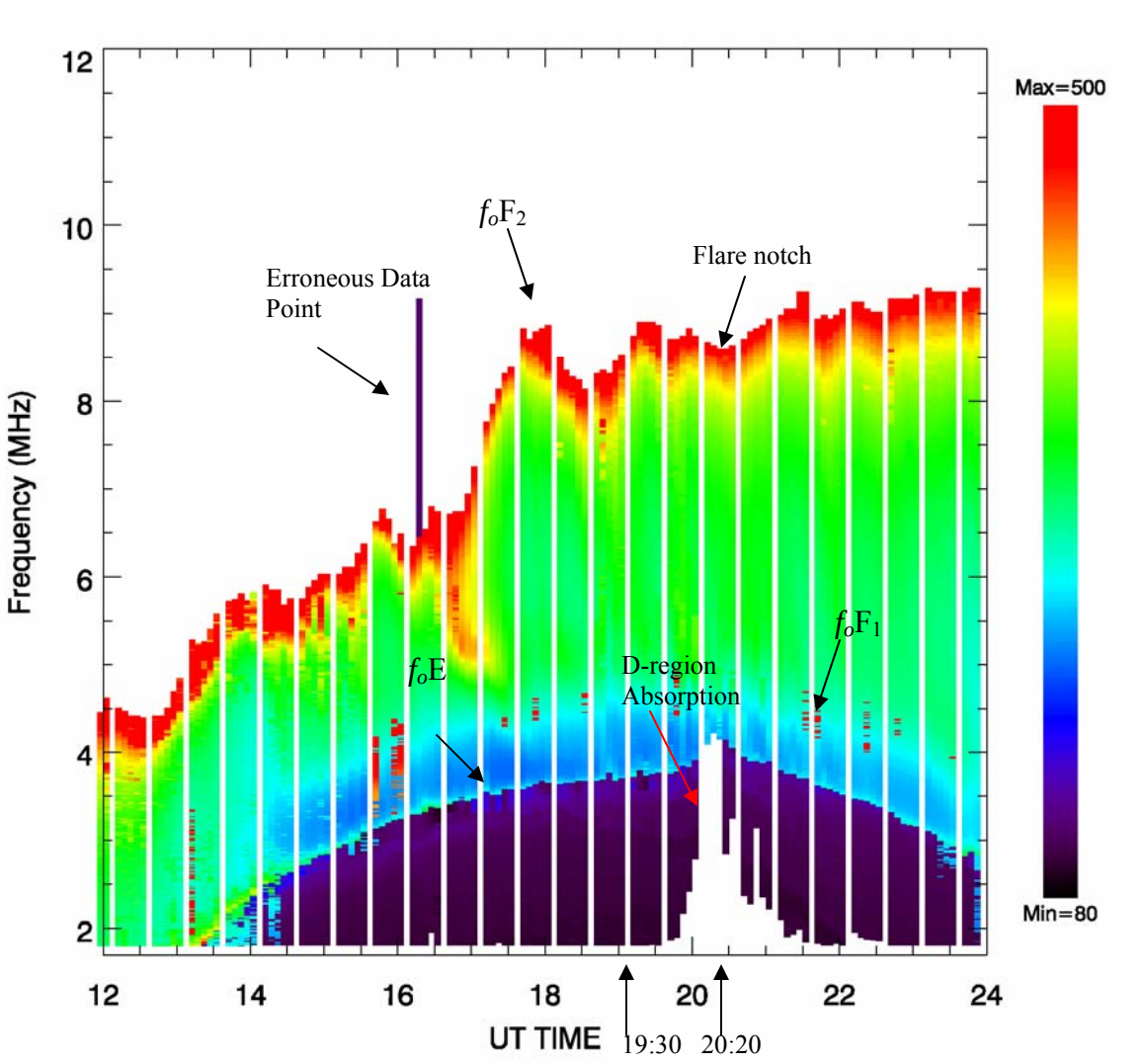

Figure 24. The figure depicts 12 hours of ionograms taken at a 5 minute cadence from Bear Lake Observatory on 4 April 2003. The ionogram is plotted as a function of signal frequency and UT time; the color scale represents the virtual height of the returned signal.

the smooth diurnal increase and decrease in frequency that is expected, but the maximum frequency is 2 MHz too large, and after the flare the frequency starts to decline when it should hold steady. This frequency peak is not due to the flare because it is also in the original TDIM output. This may indicate that the real data is varying from climatological trends and that the TDIM is unable to properly model these variances. The E and F_1

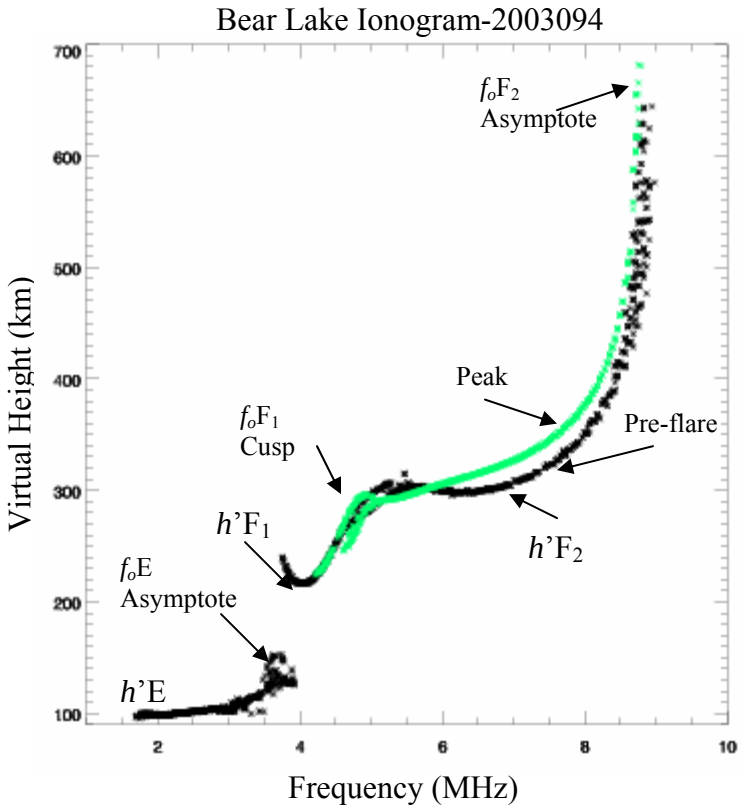

Figure 25. Ionograms for pre-flare (19:30, black) and peak flare (20:20, green) as a function of frequency and virtual height on 4 April 2003.

inversions are close to the actual data and are labeled as f_oE and f_oF_1 in the figure. In the D-region of the modeled ionograms, the white area indicates that there is no data below 100 km, but the NGDC data does extend below 100 km. There is an inverted v-notch indicating the area of D-region absorption due to the solar flare which correlates well with the real data, but there is no flare notch above the inverted v-notch as is indicated in the actual data.

The integrated model's individual ionograms (Figure 27) show the effects of the flare but the results do not accurately reflect the profiles of the NGDC ionograms. The E

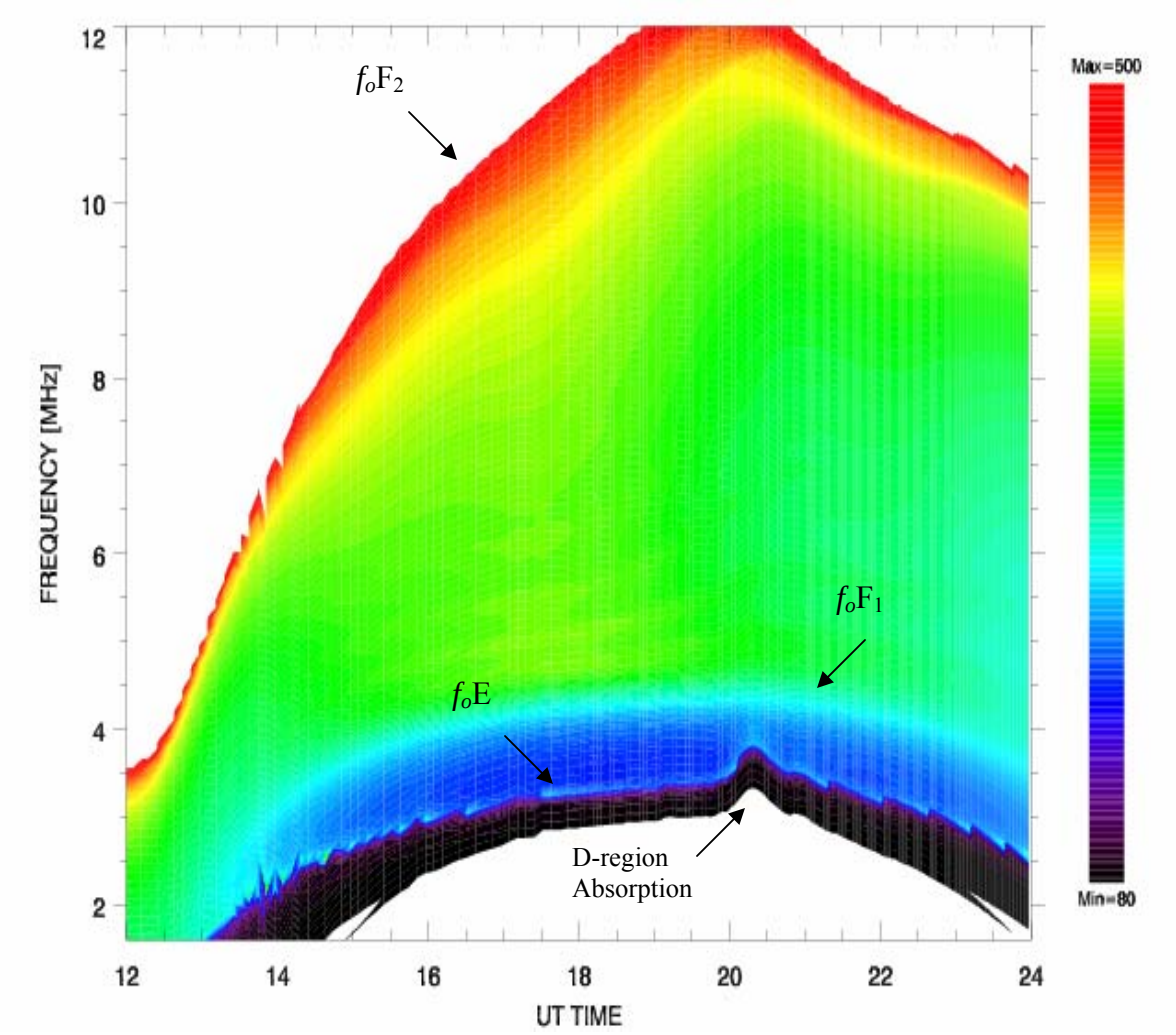

Figure 26. This figure shows a 12-hour ionogram from the integrated model for 4 April 2003.

layer density increases, but since the measured data has no information for this region it can be inferred from the composite ionograms to be approximately correct. The F layer density increases when it should decrease and the height decreases when it should increase. In the pre-flare ionogram the F_2 layer is 2 MHz too high.

Figure 28 is a contour in which a baseline file was created using a single irradiance spectrum and no flare dynamics integrated into it. Then a second file was

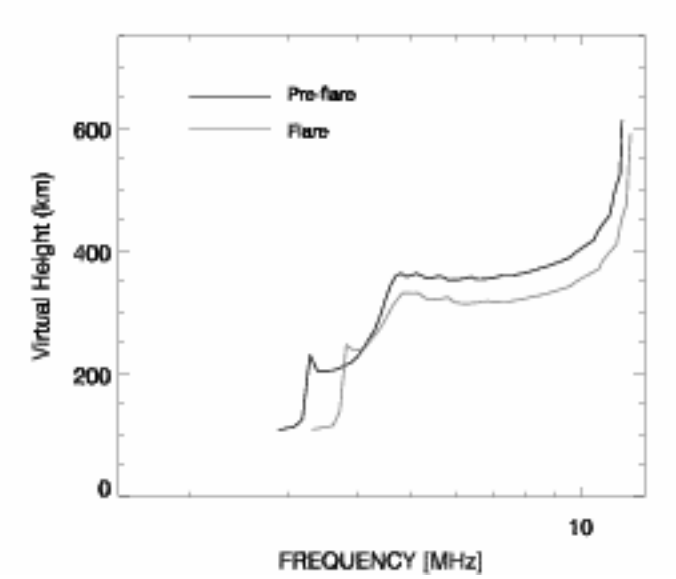

Figure 27. This figure is the integrated model pre-flare and peak flare ionograms as a function of frequency and virtual height for 4 April 2003.

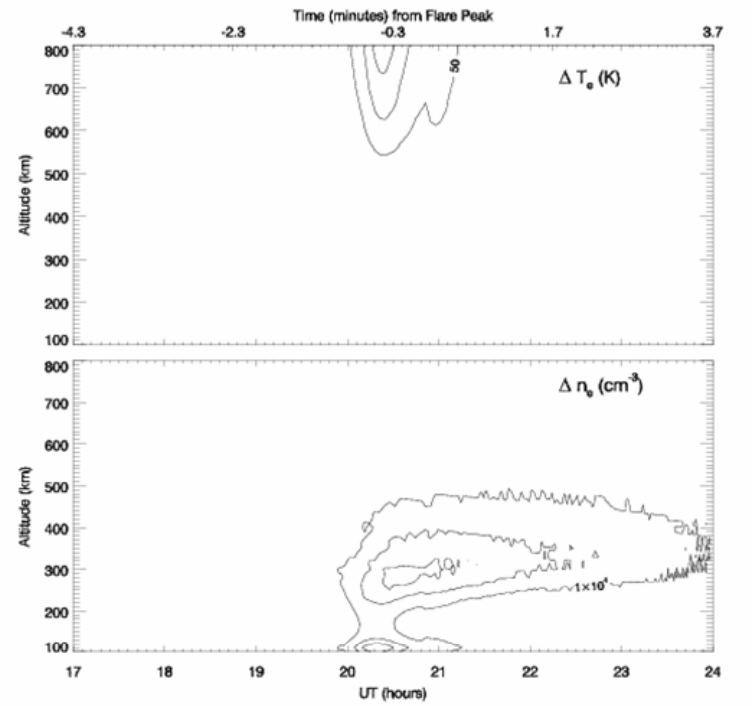

Figure 28. Flare electron density and temperature contour as a function of UT time and altitude for 4 April 2003.

created using the baseline data with the flare irradiance and beyond inserted at flare start time. This is then plotted as a contour plot to show the differences in electron density and temperature due to the flare itself. There is a slight increase in temperatures (~150 k) in the high altitudes, but as noted earlier, the increase in temperature at the middle altitudes is being suppressed. The electron densities at the lower altitudes increase as expected, but above 220 km there should be a decrease in densities not an increase as indicated in the figure.

4.2.3 Modeled Temperature and Density Profiles

The modeled electron density profile, along with the electron and ion temperature profiles, should help explain the structure of the ionograms. Looking at these details will help explain what specific change in the model is driving certain changes in the ionograms.

4.2.3.1 Baseline Profiles

This flare has a 63 minute lifetime, so the diurnal changes will be small, but still noticeable. Comparing the diurnal changes to the flare changes will show how much the model changes due to the flare input. The baseline model run is used to show how the electron density changes due to the solar zenith angle decreasing as the time progresses. Figure 29 is a plot of the electron density as a function of altitude for pre-flare and peak flare times. The F region peak drops in altitude, and as the electron temperature (Figure 30) decreases there is a simultaneous increase in electron density from 220 to 340 km. Above 340 km (F peak), photoionization does not have a strong solar zenith angle dependence so changes that are taking place here are influenced by other processes

Figure 30 shows the diurnal change of the electron and ion temperatures as a

function of altitude. The temperatures are changing, but less noticeably than the electron densities at this time of day. The electron temperature stays relatively constant above the F-peak and the ion temperature below 400 km stays the same. Above this altitude the ion temperature is controlled by the diurnal variation of the electron temperature and ion heat flow from the magnetosphere.

The diurnal changes seen here are not significant because the time advances only 50 minutes, but this will help to differentiate flare changes from diurnal changes in the integrated model profiles.

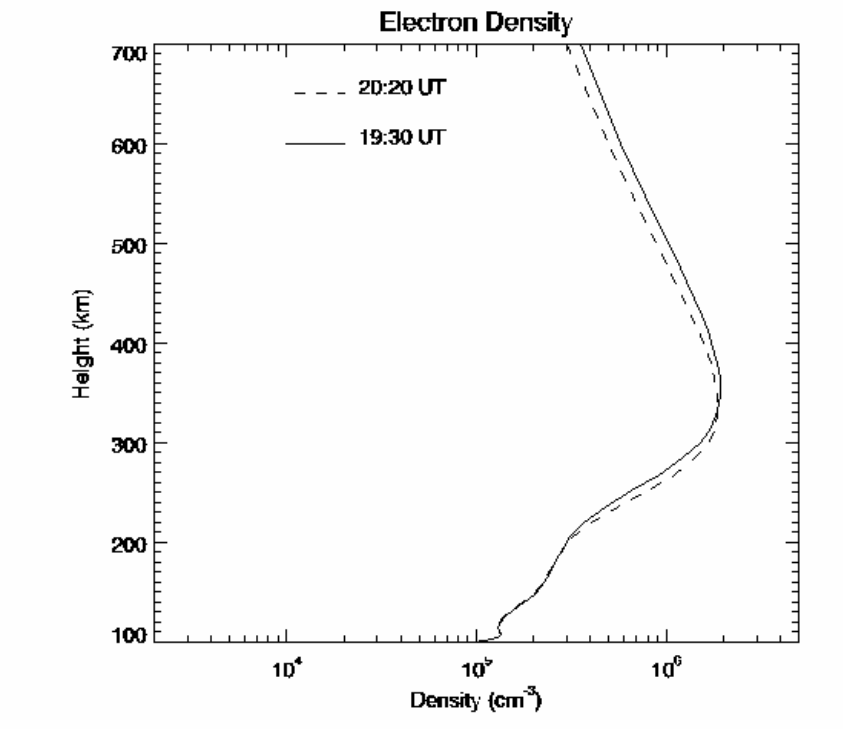

Figure 29. This figure shows how the electron density in the baseline model changes as a function of height from 19:30 UT to 20:20 UT due to diurnal variations.

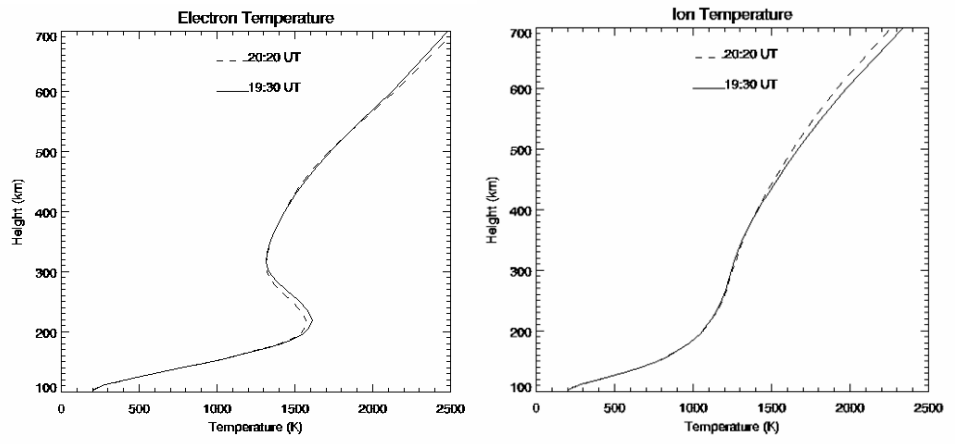

Figure 30. These figures show the electron and ion diurnal temperatures change as a function of height using the baseline model from 19:30 UT to 20:20 UT.

4.2.3.2 Integrated Model Profiles for Peak Flare

When looking at Figure 31, the integrated models electron density for pre-flare to peak flare, there is an expected density increase below 130 km, which is due to the increased ionization rate that occurs below 130 km. Figure 33 shows the pre-flare and peak flare total ionization rates as a function of altitude. The rates increase by 65% at 112 km, increasing the electron density by 26%. The density continues to slightly increase up to ~220 km due to the slight increase in total ionization rates in this region. From 220 to 700 km it has the same diurnal change in profile as seen in Figure 29. The change from baseline to flare peak is better seen in Figure 32 which is a comparison of the baseline model, at peak flare time, to peak flare electron density in the integrated model. It is obvious in this figure that the flare induced changes took place only below 220 km. A significant change in electron densities above the F peak is not expected from increased photoionization rates. But there should be a decrease in density in the F region because

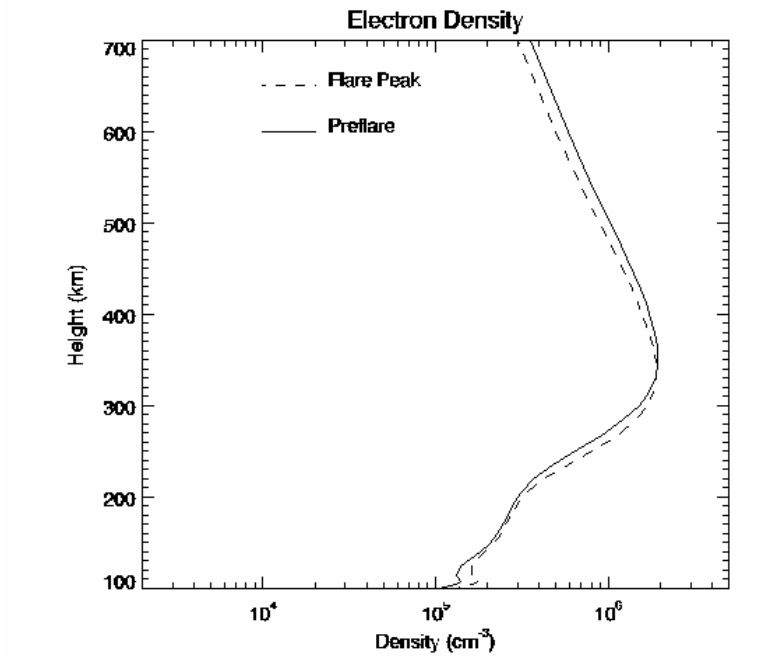

Figure 31. Pre-Flare and Flare Electron Density comparison for the Integrated TDIM model for 4 April 2003.

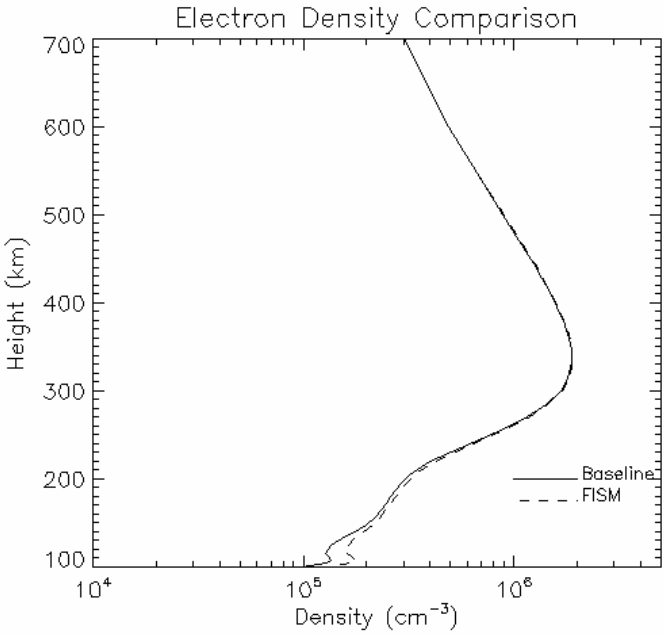

Figure 32. Flare Electron Density comparison for the baseline and Integrated TDIM model for 4 April 2003.

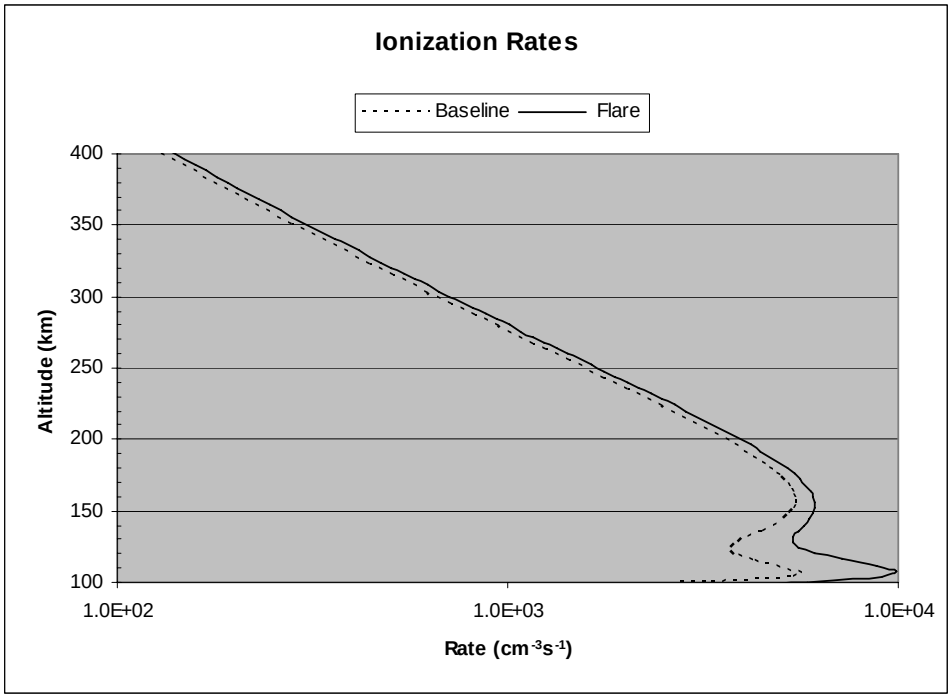

Figure 33. Total ionization rates plotted as a function of altitude for baseline and flare times. The large increase below150 km is due to the increased irradiance at short wavelengths during the flare.

of increased plasma temperatures that expand the F_2 region and force the diffusion of electrons to higher altitudes, but neither of these effects is seen in the model.

The temperature response of the integrated model is not what was expected. Figure 34 shows the electron and ion temperature change as a function of altitude for pre-flare and flare times. There should be a greater increase in electron temperature between 300 and 500 km. But the temperature here is being suppressed. There is a change in the electron temperature, ~150 K at 700 km, due to the solar flare that the integrated model does capture. This temperature increase falls short of what we expected at this time of day; according to *Sharma et al.* [2004] an approximate increase of 1.3 times over daily average or about 750 K at 700 km might be seen. The ion temperatures did not change

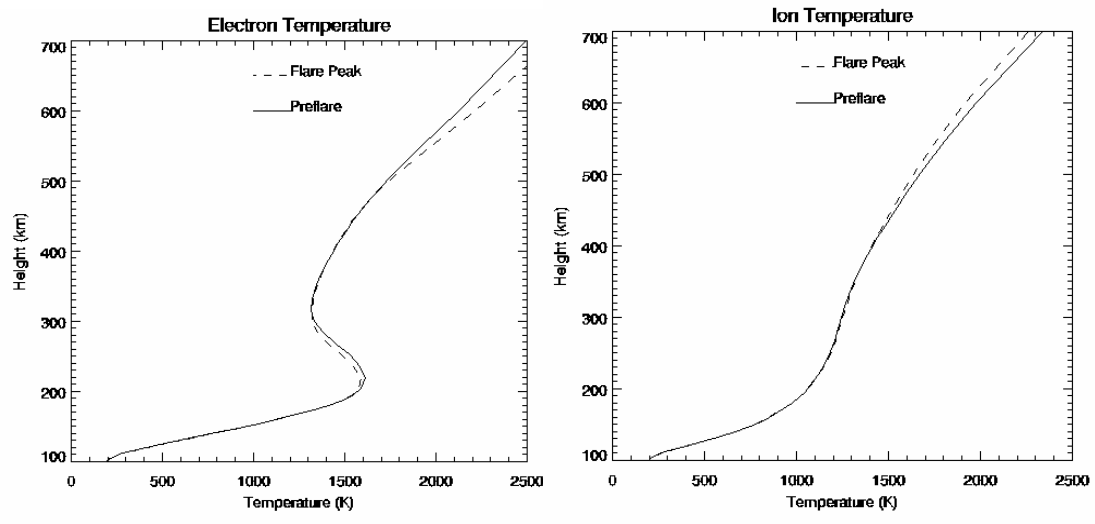

Figure 34. Pre-flare and Flare electron and ion temperature comparison for the Integrated TDIM for 4 April 2003.

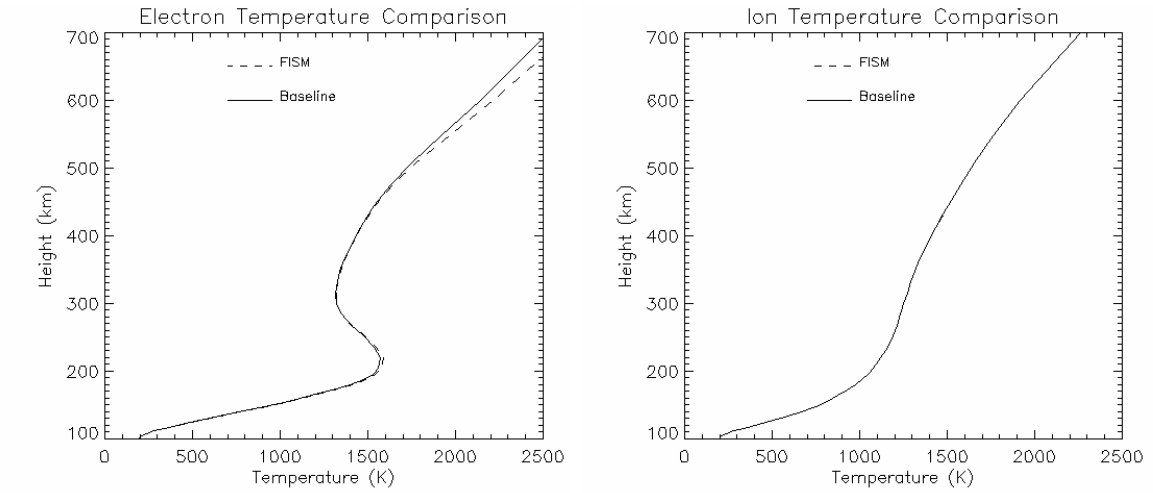

Figure 35. Flare electron and ion temperature comparison for the baseline and the integrated TDIM for 4 April 2003.

except due to the normal diurnal changes. The ion temperature should increase by 1.2 times the average or 460 K at 700 km, again according to *Sharma et al.*[2004]. Figure 35 shows the baseline compared to the integrated model for both temperatures; it is apparent in this figure that the flare had little effect on either temperature. As has been shown, the

temperature changes within the integrated model do not behave as expected when responding to the solar flare irradiance input.

The electron heating rates in Figure 36 do change significantly due to the flare irradiance. The largest increase is seen below 300 km; the peak increases by 12% while the greatest increase of 91% is seen at 108 km. These heating rates should significantly increase the electron temperature above the F_2 peak as previously shown in Equation 1.

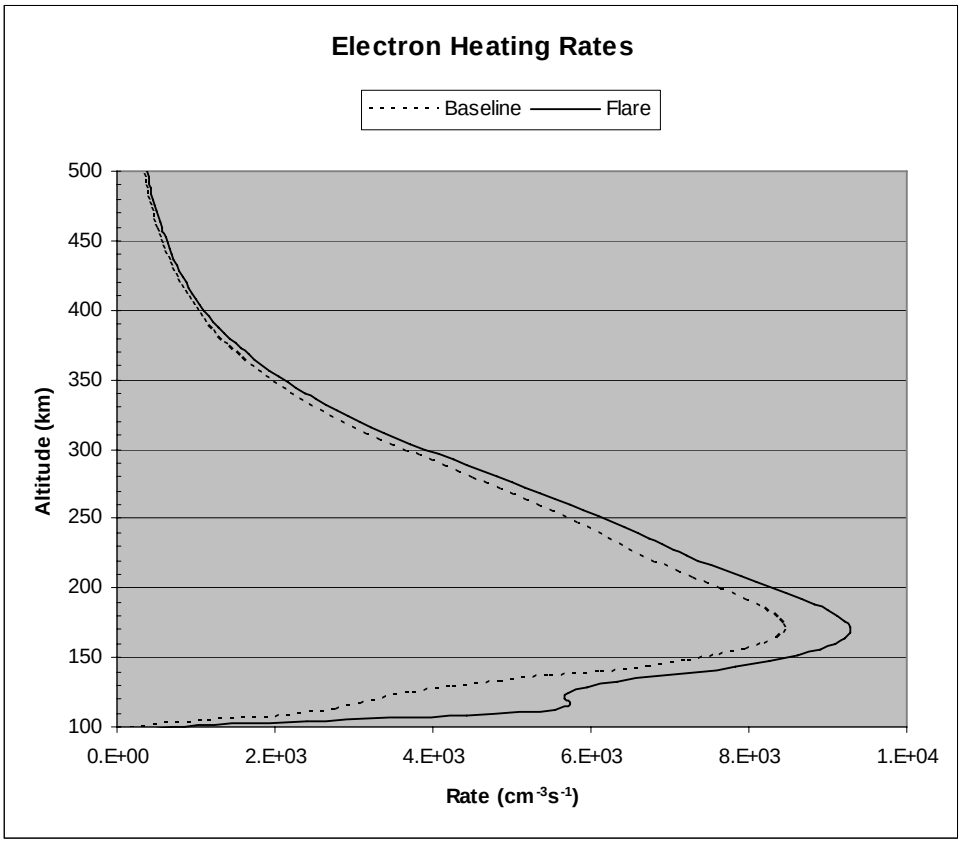

Figure 36. The integrated models electron heating rates as a function of altitude for baseline and flare.

4.2.4 FISM Spectra

The FISM spectrum is what drives the evolution of the flare over time. Figure 37 is the pre-flare solar irradiance. It is plotted in 5-nm wide wavelength bins along the x-axis and flux is shown along the y-axis. The peak flare spectrum shown in Figure 38 is different from the pre-flare spectra of Figure 37. The flare spectrum increases at all wavelengths with the greatest increase in the shortest wavelengths. Figure 39 shows the ratio of peak flare to pre-flare spectra to highlight these differences. It confirms the increase at all wavelengths with a maximum of 9.1 times the original wavelength at 50 Å. This is what causes the increase in the photoionization rates and the impact ionization rates below 120 km. The increased spectra is responsible for increasing the electron heating rates throughout the ionosphere and because the electron heating rates do increase, this does not appear to be the reason why the electron temperatures are not increasing as much as would be expected.

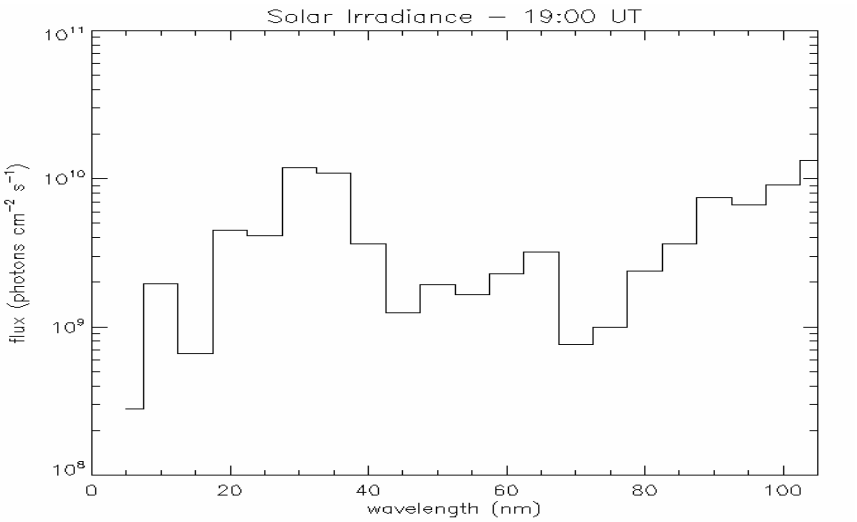

Figure 37. This is the FISM irradiance prior to flare onset used in the integrated model.

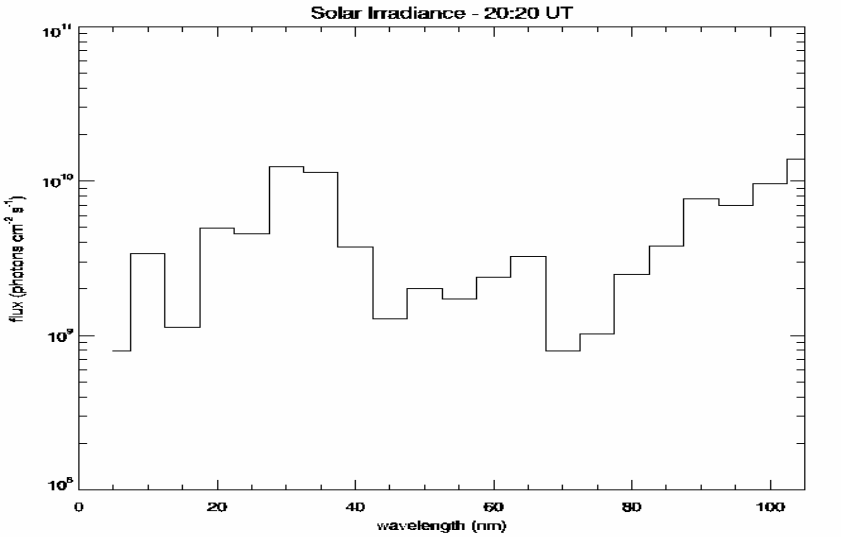

Figure 38. This figure shows the FISM irradiance during peak flare time used in the integrated TDIM model.

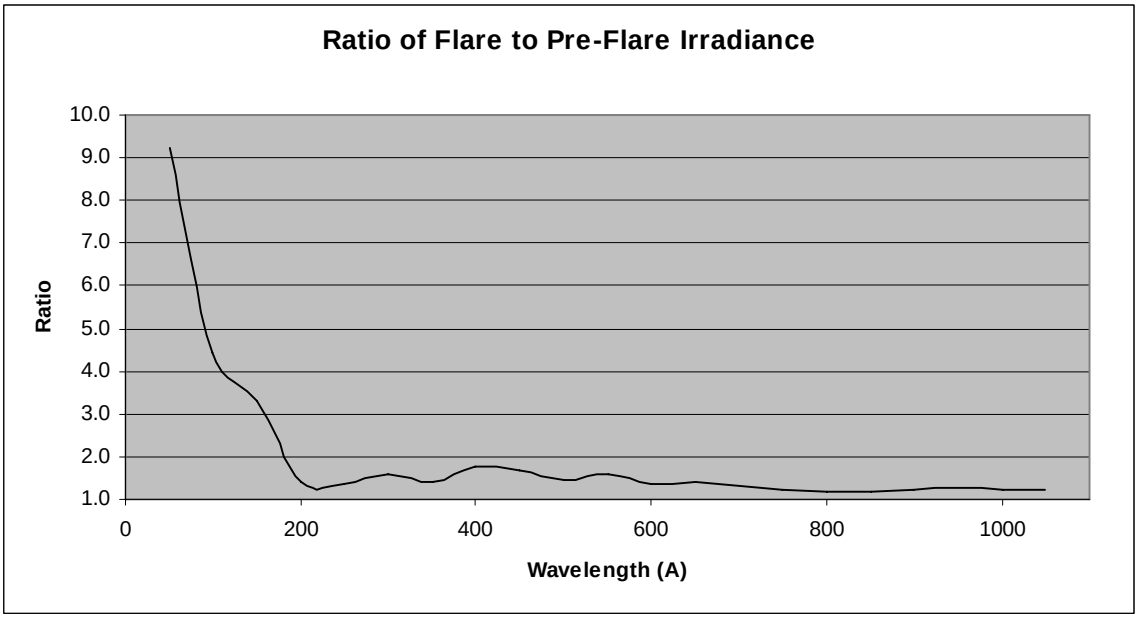

Figure 39. This graph shows the ratio of flare to pre-flare irradiance. The irradiance increases across the spectrum during the peak of the flare with the greatest increase occurring below 200 Å.

4.3 M1.1 Flare 11 May 2005

This flare began over Bear Lake Observatory at 19:23 UT (12:23 L), peaked at 19:37 UT (12:37 L) and ended at 19:54 UT (12:54 L). The solar zenith angle at peak was 24.1 degrees. Figure 40 shows a 12-hour ionogram and Figure 41 shows a single pre-flare and peak flare ionogram from Bear Lake Observatory. This is what will be used for comparison to the model runs but first an explanation of these figures.

4.3.1 Bear Lake Observatory Ionograms

The 12-hour ionogram shows normal diurnal increase in electron density starting at 1200 UT. A maximum frequency is reached at ~2100 UT on this ionogram which is due to the ionosphere relaxing back to a pre-flare state. The M1.1 flare is recognizable by the inverted v-notch due to D-region absorption from ~19:30 UT to ~20:00 UT. Note that this flare also has a flare notch located above the inverted v-notch. The f_oE, f_oF_1 and f_oF_2 regions are identified on the figure. The two arrows at the bottom of the figure indicate the times of the ionograms in Figure 41.

The ionograms in Figure 41 where taken at 19:15 UT (black) and 19:35 UT (green). They are plotted as a function of virtual height and frequency. The bases of the black cusps in this figure indicate h'E at ~100 km, h'F_1 at ~240 km, and h'F_2 at ~320 km. The h'F_2 increases to ~350 km at peak flare. The E region densities increase slightly, while the F_1 region densities remain the same up to the f_oF_1 cusp. Beyond this, the electron densities decrease, as is expected with a flare notch.

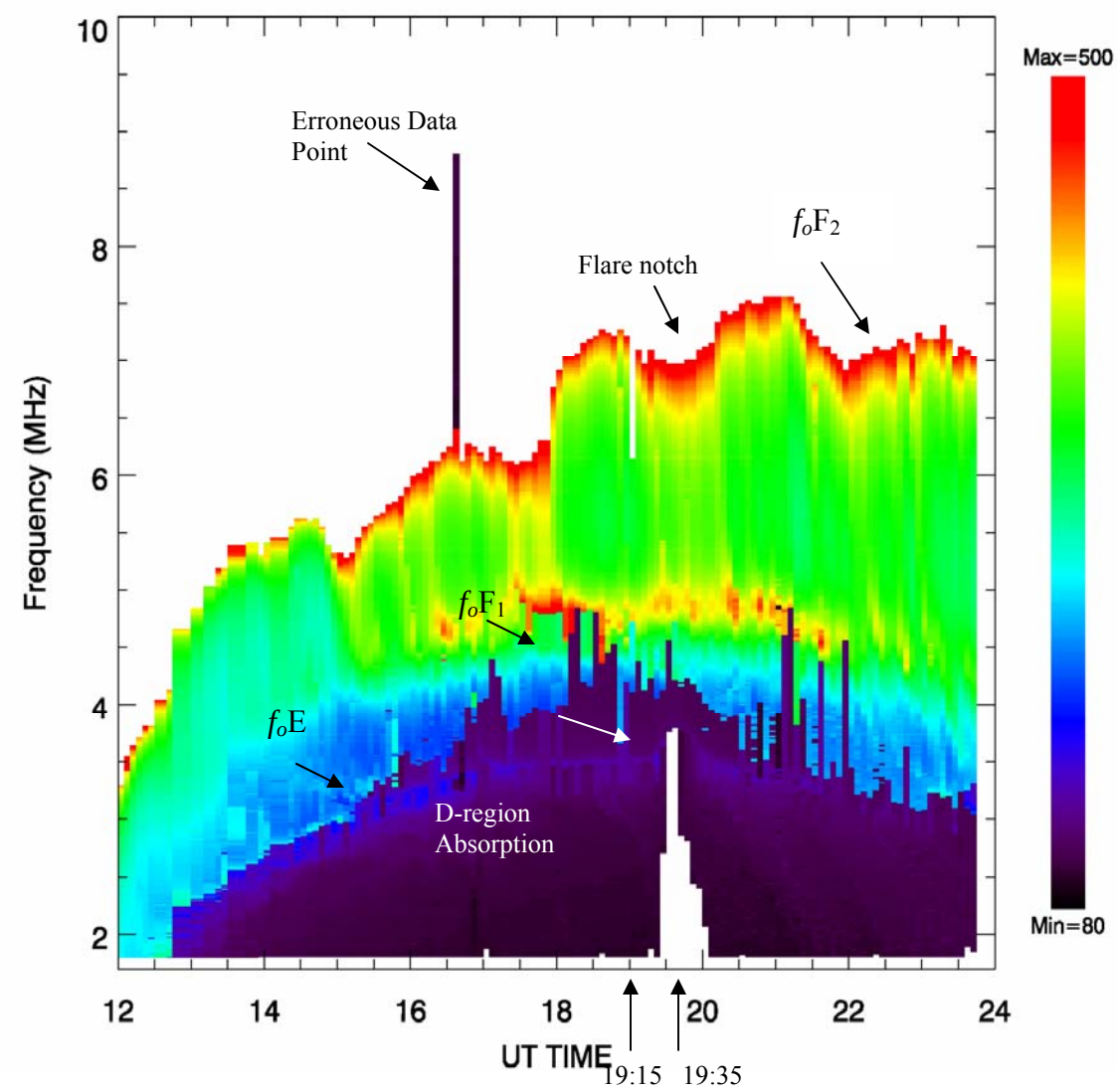

Figure 40. The figure depicts 12 hours of ionograms taken at a 5 minute cadence from Bear Lake Observatory on 11 May 2005. The ionogram is plotted as a function of signal frequency and UT time; the color scale represents the virtual height of the returned signal.

4.3.2 Integrated Model Ionograms

Like the first flare, the integrated model will be compared to the actual NGDC data. Once again the modeled ionograms in Figure 42 shows the smooth diurnal increase and decrease in frequency that is expected, but again, the maximum frequency is 2 MHz

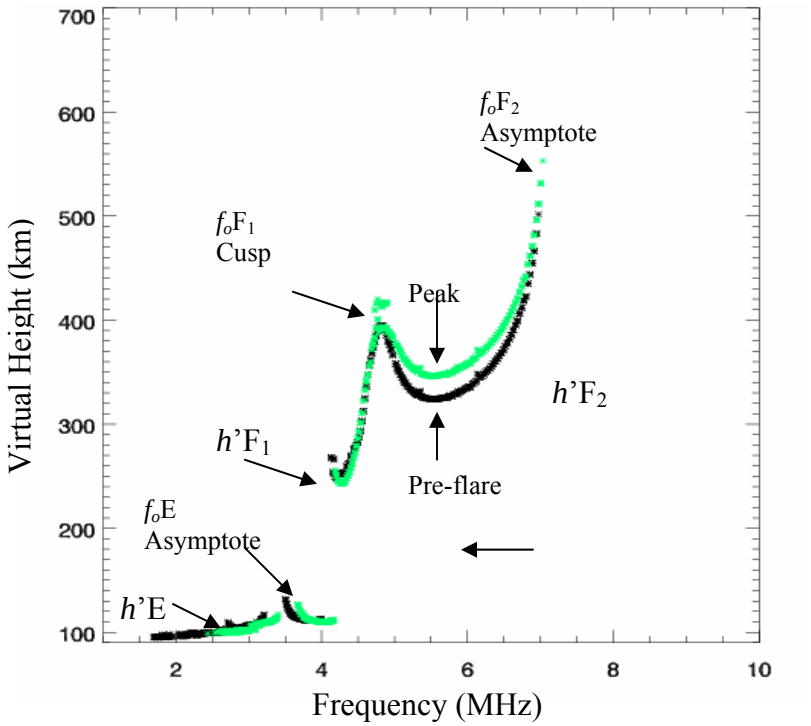

Figure 41. The figure shows ionograms for pre-flare (19:15, black) and peak (19:35, green) on 11 May 2005. These are plotted as a function of frequency and virtual height.

too large. The height of the E and F_1 inversions are close to the actual data. There is an inverted v-notch at the correct time but there is no flare notch above it.

The integrated model ionograms, in Figure 43, show that the f_oF_2 asymptote is too high. It approaches 11 MHz when the actual data is showing 7 MHz. The E region data is also showing an increase in frequency when the actual data does not significantly change. The F region does not change and since there is only 30 minutes between the two ionograms, there would also be no noticeable diurnal changes.

The electron density and temperature contour in Figure 44 is similar in characteristic to Figure 28 of the first flare. There is again a slight increase in

temperature at upper altitudes with no change in mid-altitudes and slight changes in the lower altitudes. The densities increase below 120 km with a slight increase up to 500 km. There should be a decrease at the F_2 peak (~300 km), but this is once again not being modeled as expected.

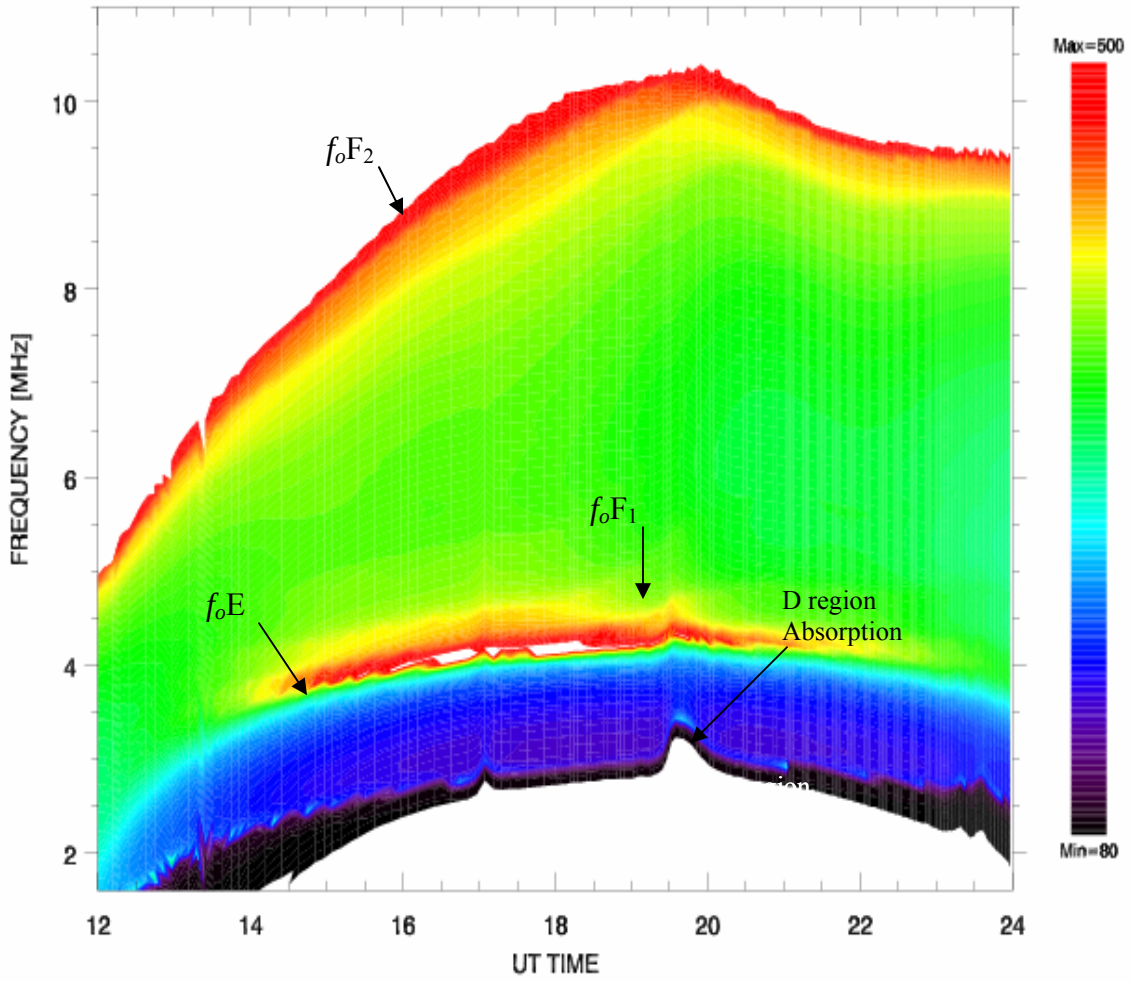

Figure 42. This figure shows a 12-hour ionogram as a function of UT time and frequency, from the integrated model for 11 May 2005.

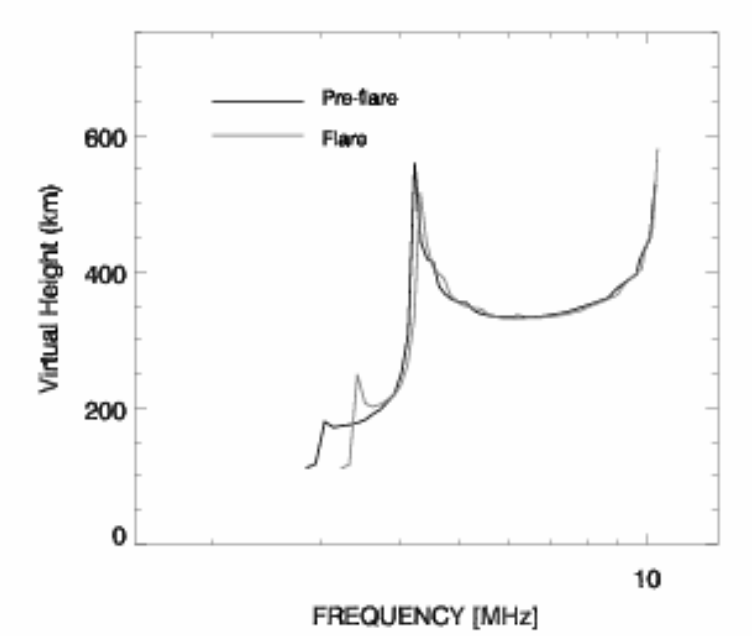

Figure 43. This figure shows the integrated model pre-flare and peak flare ionograms as a function of frequency and virtual height for 11 May 2005.

4.3.3 Modeled Temperature and Density Profiles

The modeled electron density profile, along with the electron and ion temperature profiles, should help explain the structure of the ionograms. Looking at these details will help explain what may be driving the incorrect temperature and density values in the ionograms.

4.3.3.1 Baseline Profiles

The baseline density and temperature profiles are presented to show what diurnal changes occur. Since the time between pre-flare and peak flare is only 20 minutes, there will not be a significant change in these parameters. Figure 45 shows the electron density profile with minimal changes. Looking at Figure 46 you can see that the electron and ion temperatures will not change with only 20 minutes between data points. So any change between pre-flare and flare profiles will be solely due to the flare input.

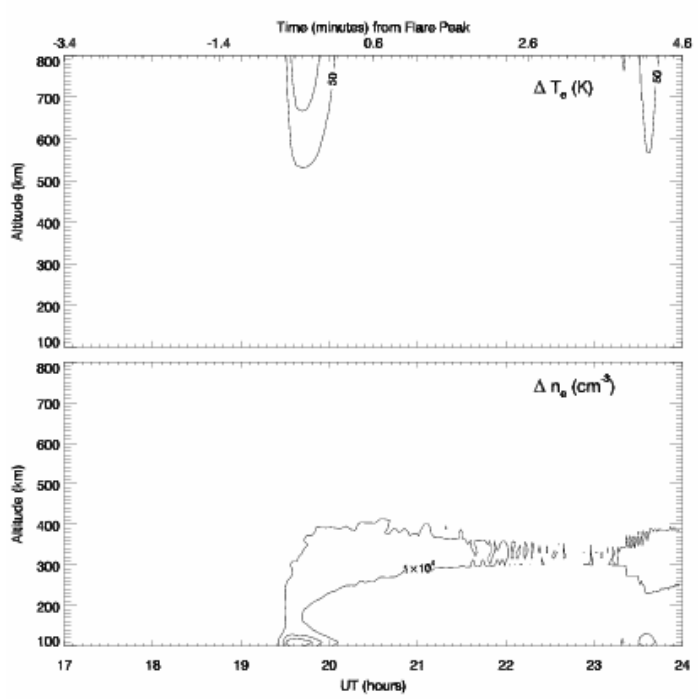

Figure 44. Flare electron density and temperature contour plotted as a function of UT time and altitude, for 11 May 2005.

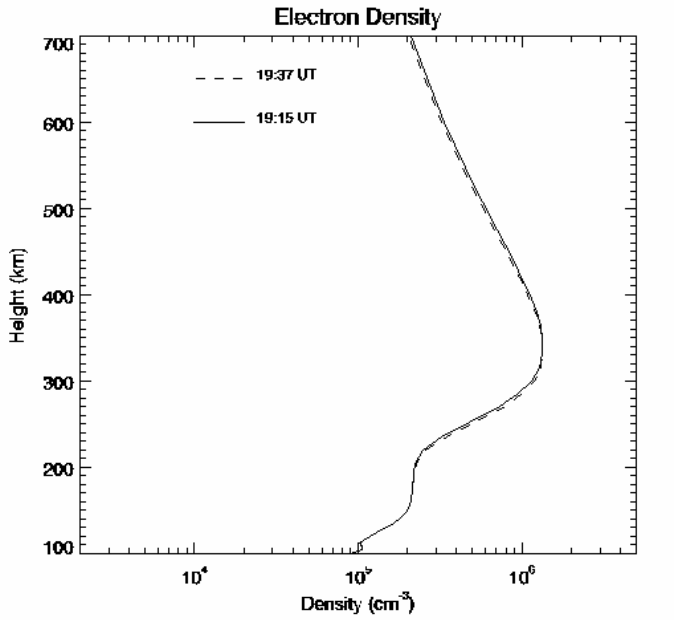

Figure 45. This figure shows the diurnal changes of the electron density using the baseline model from 19:15 UT to 19:37 UT.

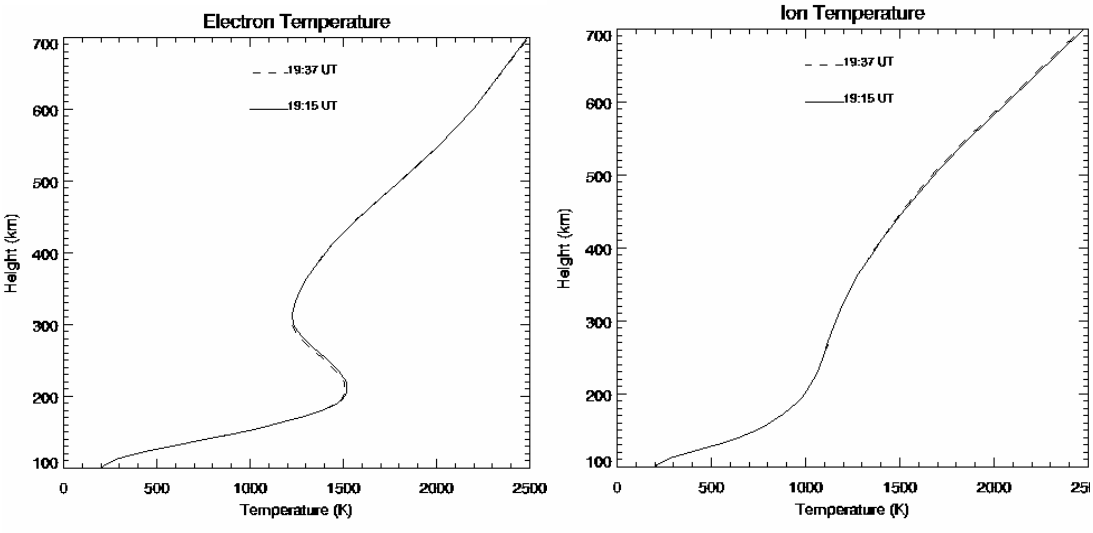

Figure 46. These figures show the electron and ion diurnal temperature change as a function of altitude using the baseline model.

4.3.3.2 Integrated Model Profiles

When looking at Figure 47, the only notable change between the pre-flare and peak flare electron density profile is below 140 km, which is due to the increased ionization rate below 140 km. Figure 48 shows the total ionization rates for baseline and peak flare as a function of altitude. The greatest increase in ionization is 93% at 108 km, which increases the electron density by 32%. From 140 to 230 km there is a slight increase in density and then beyond 230 km the profile matches the slight diurnal change in Figure 45. There should have been a decrease in electron densities at the F_2 peak (~330 km) but it is not seen in this density profile.

There is even less of a temperature response in this flare than the previous flare. The integrated model does not accurately represent the temperature response between pre-flare and peak flare times; an increase in electron temperature from 230 to 700 km. Figure 50 shows a very slight increase in electron temperature beyond 500 km and no

change in ion temperature. Looking at Figure 51 confirms that there is no significant change due to the flare. As with the previous flare, this flare is also not increasing in temperature as would be expected. For both the ion and electron temperatures there should be a 1.3 and 1.2 times the daily average temperature increase respectively. If this increase would occur, then the flare notch that is expected to be seen on the 12-hour ionogram would appear.

The electron heating rates in Figure 52 do change but with a slightly different profile than the previous flare. The largest increase for this flare is below 300 km; the peak increases by 10% while the greatest increase is 2.5 times the original heating rate at 108 km. These heating rates should significantly increase the electron temperature above the F_2 peak.

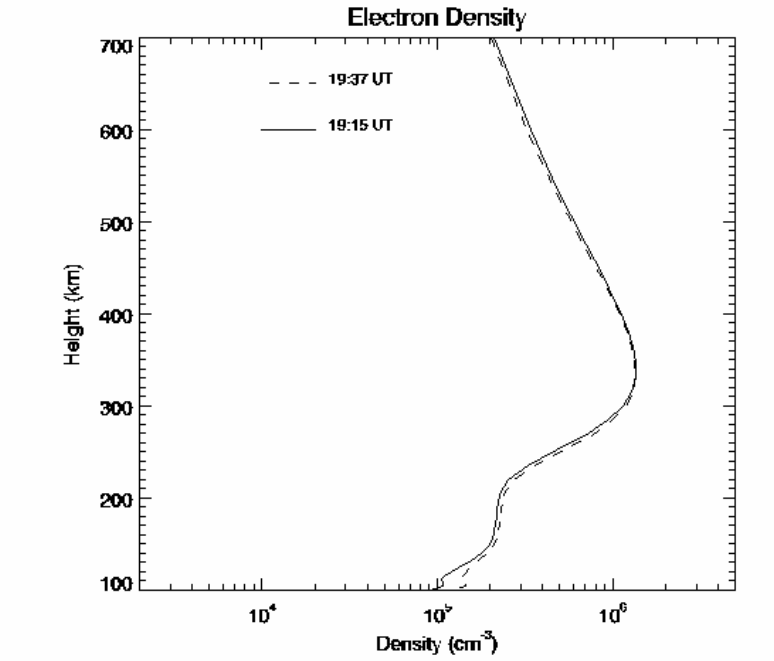

Figure 47. Pre-flare and peak flare electron density comparison for the integrated model, plotted as a function of altitude for 11 May 2005.

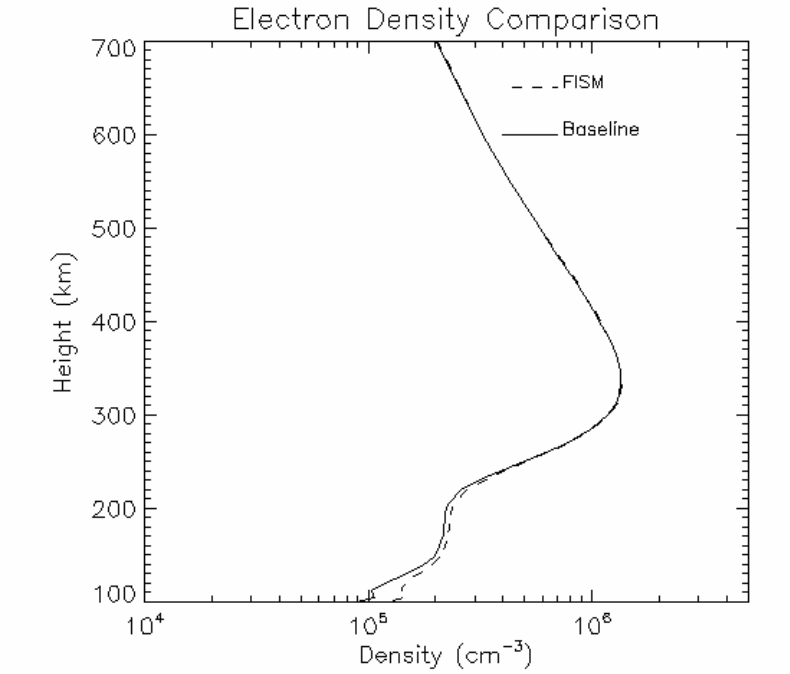

Figure 48. Peak flare electron density comparison for the baseline and integrated model, plotted as a function of altitude for 11 May 2005.

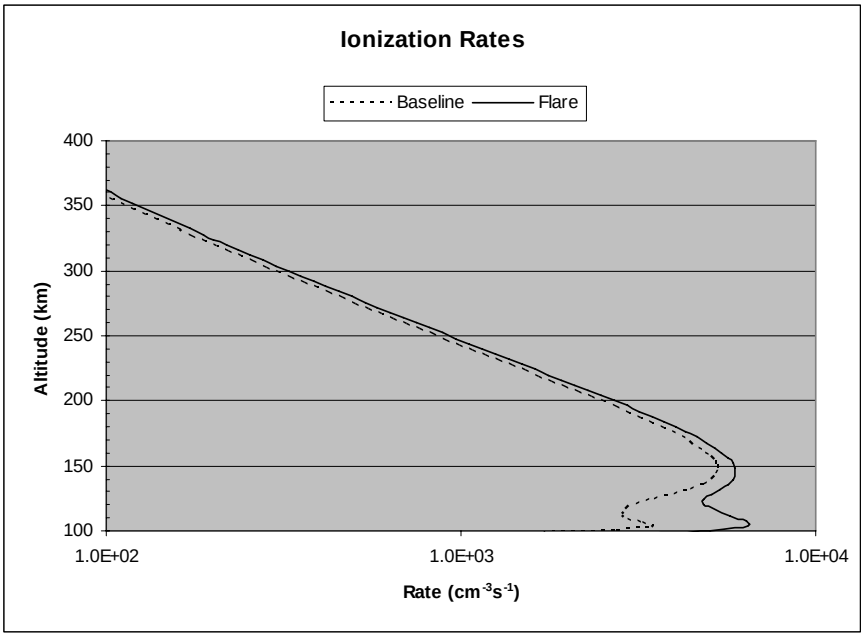

Figure 49. Total ionization rates plotted as a function of altitude for baseline and peak flare. The large increase below 150 km is due to the increased irradiance at short wavelengths during the flare.

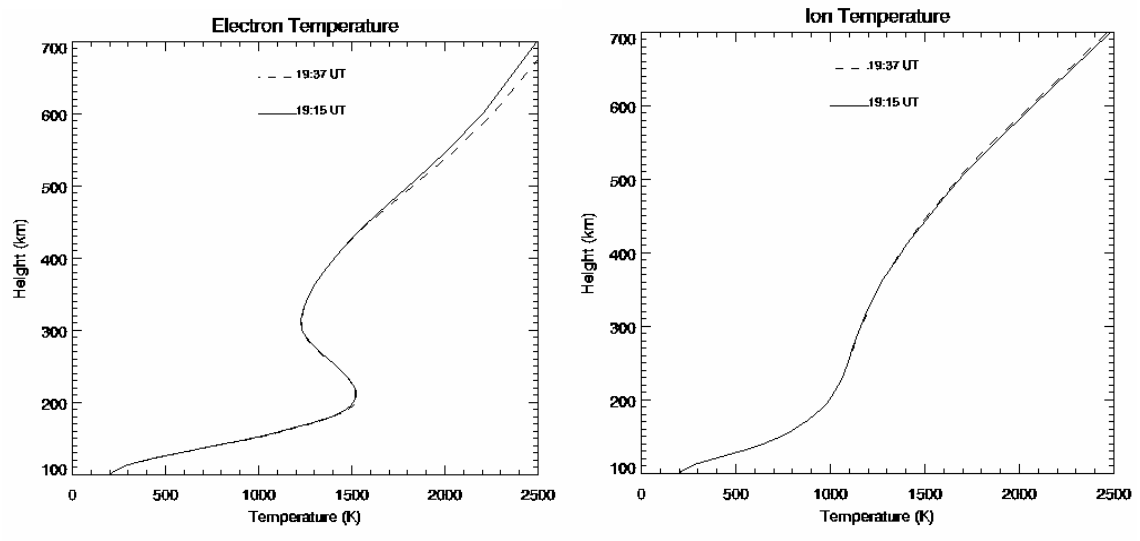

Figure 50. Pre-flare and flare electron and ion temperature comparison for the integrated TDIM for 11 May 2005.

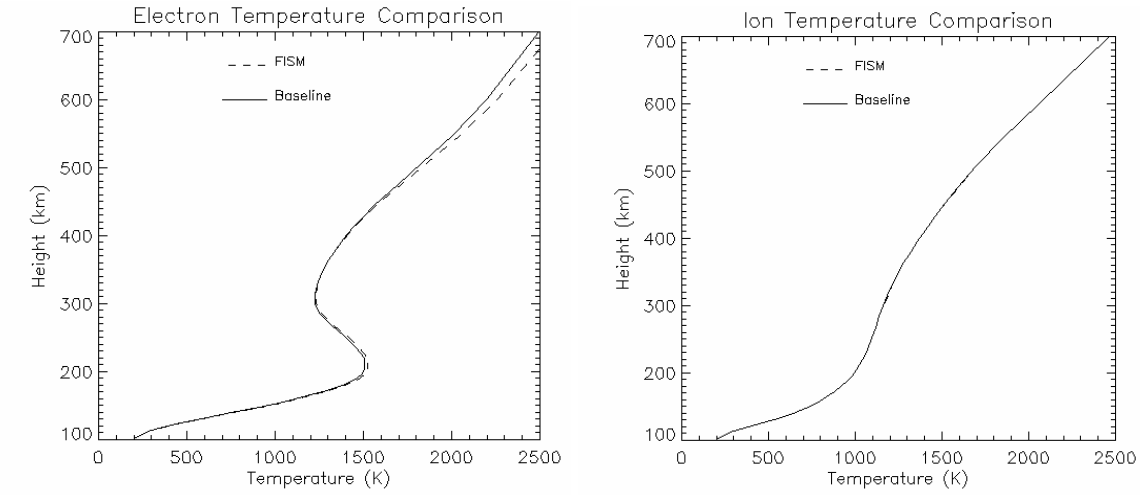

Figure 51. Peak flare electron and ion temperature comparison for the baseline and integrated TDIM for 11 May 2005.

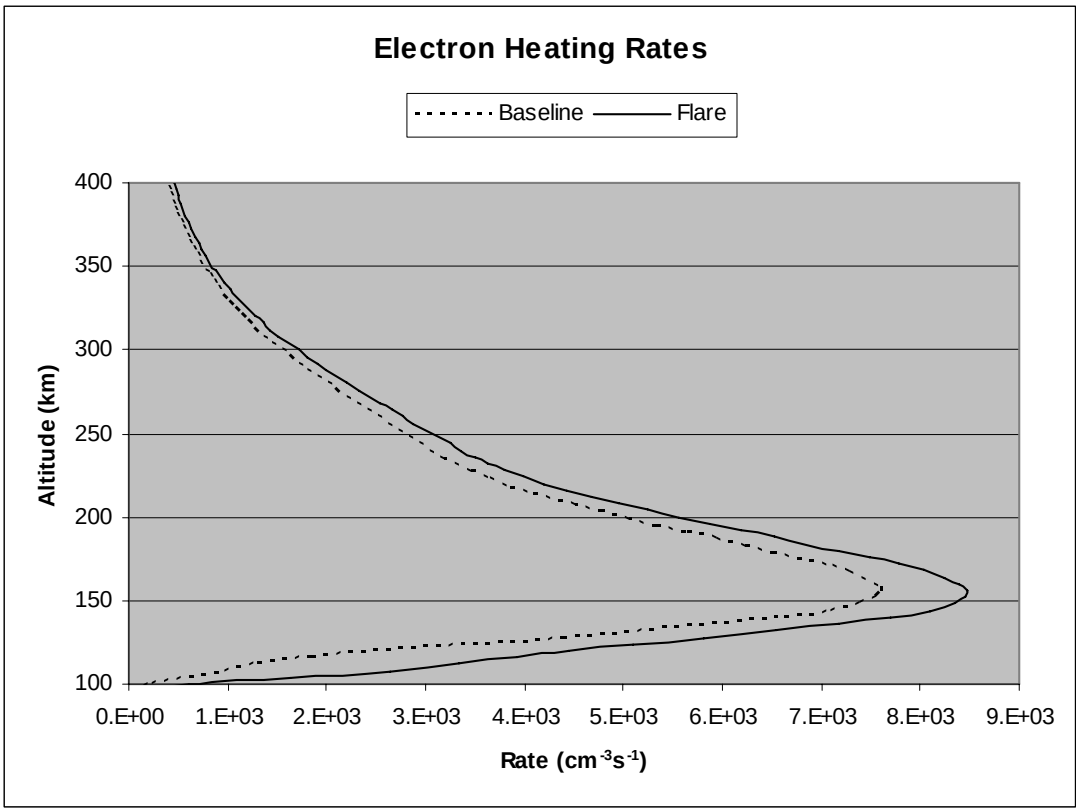

Figure 52. The integrated models electron heating rates as a function of altitude for pre-flare and peak flare times.

4.3.4 FISM Spectra

The pre-flare spectrum is in Figure 53. The wavelength in this figure is plotted in 5 nm wide bins as a function of flux. Figure 54 is the peak flare spectrum which has increased from the pre-flare spectrum across all wavelengths. Figure 55 shows the ratio of peak flare to pre-flare spectra. It confirms a very slight increase beyond 200 Å. At wavelengths less than 200 Å there is a large increase with a maximum of 4.7 times the original wavelength at 50 Å. The increase in the peak flare spectrum is what causes the increase in photoionization and impact ionization rates below 140 km while also increasing the electron heating rates.

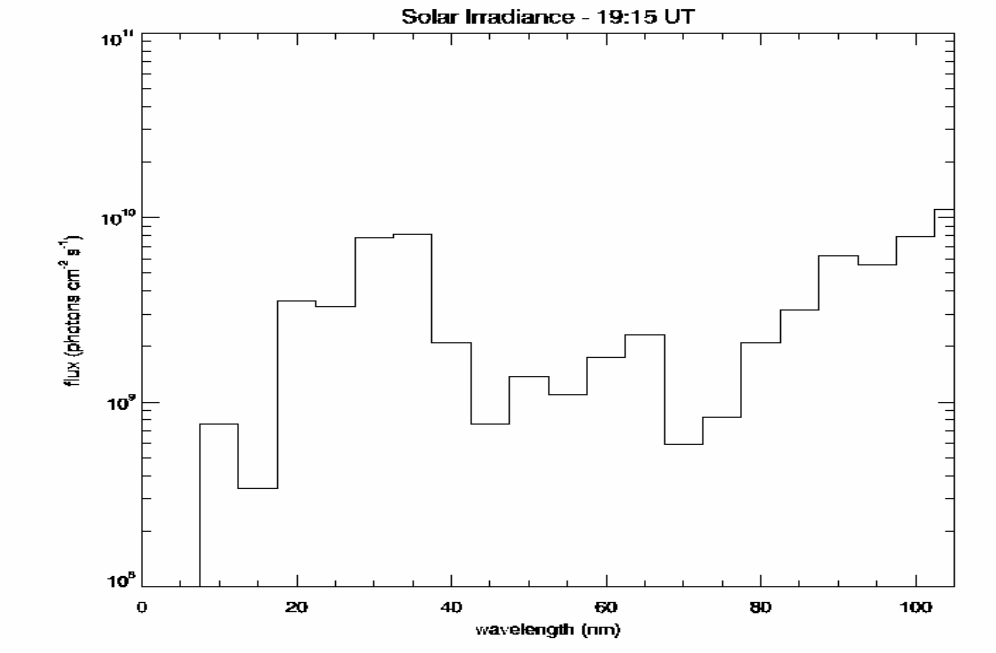

Figure 53. This is the FISM irradiance prior to flare onset used in the integrated model. The wavelength is plotted in 5 nm wide bins as a function of flux.

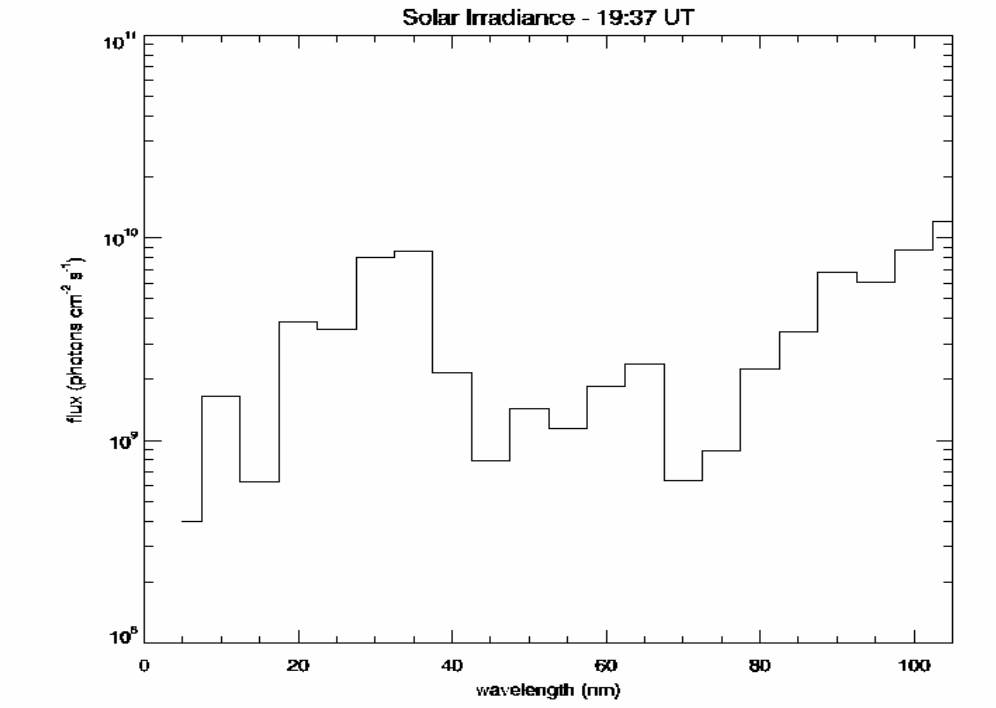

Figure 54. This is the FISM irradiance at flare peak used in the integrated model.

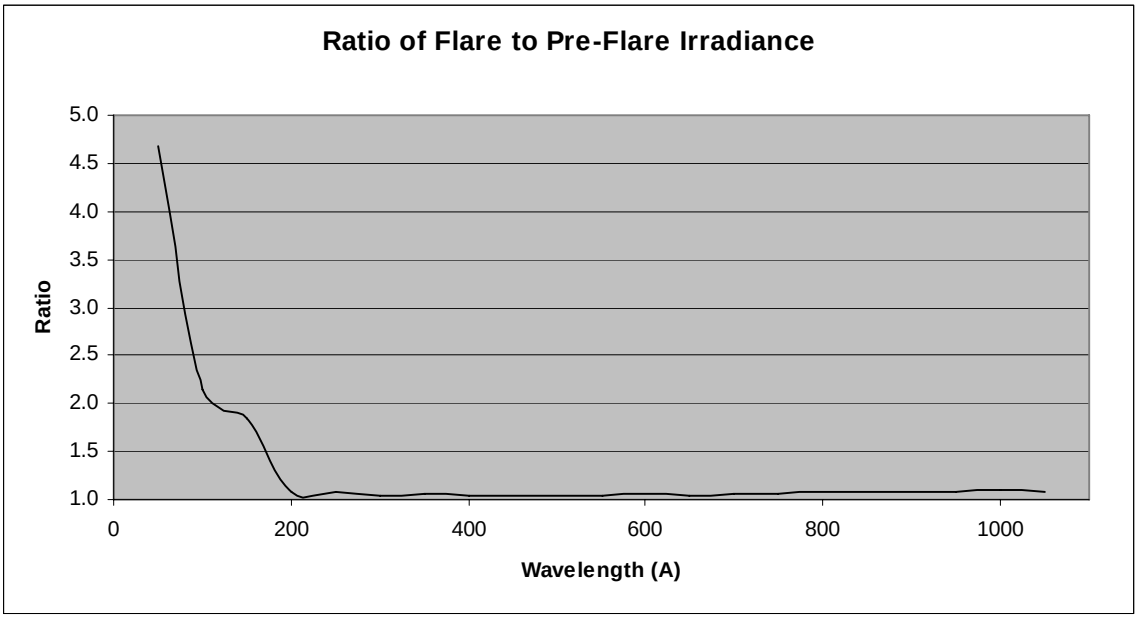

Figure 55. This graph shows the ratio of flare to pre-flare irradiance. The irradiance increases significantly only up to 200 Å.

V. Conclusions and Future Work

5.1 Conclusions

The objective of this thesis was to use a current, well tested model of the quiet ionosphere and integrate a more rigorous development of certain parameters so that a flare time response of the ionosphere could be modeled. We achieved this in the E and lower F region, but beyond this point the model failed to fully develop the ionospheric response expected. In trying to understand where the problem may be, a discussion of what happened with each changed parameter and how it affected the outcome of each model will follow.

Starting with the FISM model, the irradiances used to describe the solar variations worked very well. The model was able to easily integrate the flare effects into the lower ionosphere and the spectra increased at the expected wavelengths. This increase in irradiance values caused the photoionization and electron impact ionization to increase in the lower ionosphere; this effect was especially strong during the flare.

The Glow model integration appeared to be correct. There were two major changes in the program. First the photoionization rates were replaced with Glow values and the Glow electron impact ionization rates were added to the photoionization rates. The photoionization and electron impact ionization rates had correct magnitude ranges. The profile structure was also correct. Referring back to Figures 5 and 6, you can see the profiles of this ionization which correlates well to other documented studies of this structure. I do not believe this was the problem with the model. The next major change

from the Glow program involved the electron heating rates. The heating rates increased as they should have with pre-flare and peak flare values.

The thermal structure of the ionosphere was not what was expected beyond 220 km in both flares. The thermal structure from 220 to about 500 km followed the diurnal changes expected for these quantities. Above 500 km there was an increase in electron temperature but it fell significantly short of the expected values (100 K vs. 750 K). Since the temperatures did not get modeled appropriately, the electron densities never decreased at the F_2 peak, which prevented the flare notch from developing. The ion temperatures followed diurnal patterns completely; no change due to flaring was noted. So where did the model go wrong?

The TDIM is a very complicated model that has been developed and changed since 1988; it is very possible that there is code that manipulates the temperatures in unexpected ways. This model was not originally written to include the effects of flares, so it is possible that in trying to keep out data that would be erroneous for a quiet solar day it is suppressing the effects of the flare.

Even though the electron and ion temperature profiles were incorrect above 220 km, the lower E and F region did respond as expected. The success of using the irradiance from FISM and the total ionization rates and electron heating rates from Glow gets us one step closer to understanding the effects that flares have on the ionosphere.

5.2 Future Work

Trying to find out why the electron and ion temperatures were not correctly calculated during the flare will be the next step. This would have to start with the original programmers and scientists from Utah State University. With their insight, this

problem may quickly be resolved. Once this issue is resolved and the model is validated against NGDC data, one would be able to study the effects that flares will have on the ionosphere and possibly use this as a forecasting tool.

Bibliography

Bailey, Scott M., Charles A. Barth, Stanley C. Solomon. 'A model of nitric oxide in the lower thermosphere," *J. Geophys. Res*., 107(A8), 1205, doi: 10.1029 /2001JA000258, 2002.

Chamberlin, Phil. PhD Thesis, Chapter 2 – Solar Irradiance Modeling and Chapter 6 – Flare Irradiance Spectral Model Algorithms (Draft Copy), University of Colorado, 2005.

Hedin, A. E. "Extension of the MSIS thermosphere model into the middle and lower atmosphere," *J. Geophys. Res.,* 92: 1159, 1991.

Hinteregger, H. E. "Observational, reference and model data on solar EUV, from measurements on AE-E," *J. Geophys. Res.,* 8:1147, 1981.

Huba J. D., H.P. Warren, G. Joyce, X. Pi,B. Iijima and C. Coker. "Global Response of the Low-latitude to Midlatitude Ionosphere Due to the Bastille Day Flare," *Geophys. Res*. 32, L15103, 2005.

Meier R.R., H. P. Warren, A. C. Nicholas, J. Bishop, J. D. Huba, D.P. Drob, J. L. Lean, J. M. Picone, J. T. Mariska, G. Joyce, D. L. Judge, S. E. Thonnard, K. F. Dymond and S. A. Budzien. "Ionospheric and dayglow responses to the radiative phase of the Bastille Day flare," *Geophys. Res*. *Lett.*, 29(10), 1461, doi: 10.1029/2001GL013956, 2002.

Nagy, A. F., and P. M. Banks, "Photoelectron fluxes in the ionosphere," *J. Geophys. Res.* 75, 6260, 1970.

"National Space Weather Strategic Plan," FCM-P30-1995, www.ofcm.gov/nswp-sp/text/a-cover.htm

Richards, P.G., and D. G. Torr. "Ratios of photoelectron to EUV ionization rates for aeronomic studies," *J. Geophys*. Res., 93(A5), 4060, 1988.

Richards, P.G., J. S. Fennelly, and D. G. Torr. "EUVAC: A solar EUV flux model for aeronomic calculations," *J. Geophys*. Res., 99(A5), 8981, 1994.

Schunk, R.W. "A mathematical model of the middle and high latitude ionosphere," *PAGeoph*., 127(2/3), 255, 1988.

Schunk Robert W. and Andrew F. Nagy. *Ionospheres: Physics, Plasma Physics, and Chemistry*. Cambridge: Cambridge University Press, 2000.

Sharma D. K., J. Rai, M. Israil, P. Subrahmanyam, P.Chopra, and S.C. Garg. "Enhancement in Electron and Ion Temperatures due to Solar Flare as Measured by SROSS-C2 Satellite," *Annales Geophysicae* 22: 2047, 2004.

Smithtro, C. G., T. Berkey, D. Thompson, J.J. Sojka, and R.W. Schunk. "Observation and Modeling of Mid-Latitude Ionospheric Dynamics during Solar X-Ray Flares," Air Force Institute of Technology, 2004.

Solomon, Stan. "Preliminary Documentation for the Glow Model," University of Colorado, April 2005.

Titheridge J. E. "Direct alllownace for the effect of photoelectrons in ionospheric modeling," *J. Geophys. Res*., 101:357, 1996.

Tsurutani, B. T., D. L. Judge, F. L. Guarnieri, P. Gangopadhyay, A. R. Jones, J. Nuttall, G.A. Zambon, L. Didkovsky, A. J. Mannucci, B. Iijima, R. R. Meier, T. J. Immel, T. n. Wooods, S. Prasad, L. Floyd, J. Huaba, S. C. Solomon, P. Straus, and R. Viereck. "The October 28, 2003 Extreme EUV solar flare and resultant extreme ionospheric effects: Comparison to other Halloween events and the Bastille Day event," *Geophys Res. Lett.,* 32: L03S09, 2005.

Woods, T. N., Scott M. Bailey, W. K. Peterson, Stanley C. Solomon, Harry P. Warren, Francis G. Eparvier, Howard Garcia, Charles W. Carlson and James P. McFadden "Solar extreme ultraviolet variability of the X-class flare on 21 April 2002 and the terrestrial photoelectron response," *Space Weather*, 1(1), 1001, doi: 10.1029/2003SW060010, 2003.

Zhang, D. H., Z. Xiao, K. Igarashi, and G.Y. Ma. "GPS-derived ionospheric total electron content response to a solar flare that occurred on 14 July 2000," *Radio Sci*., 37(5), 1086, doi; 10.1029/2001RS002542, 2002.

REPORT DOCUMENTATION PAGE

Form Approved
OMB No. 074-0188

1. REPORT DATE *(DD-MM-YYYY)*	**2. REPORT TYPE**	**3. DATES COVERED** *(From – To)*
03-23-2006	**Master's Thesis**	Sep 2005 – Mar 2006

4. TITLE AND SUBTITLE

Modeling E & F Region Ionospheric Response to X-Ray Solar Flares

5a. CONTRACT NUMBER

5b. GRANT NUMBER
2006-064

-5c. PROGRAM ELEMENT NUMBER

6. AUTHOR(S)

Parsons, Annette M., 1Lt, USAF

5d. PROJECT NUMBER

5e. TASK NUMBER

5f. WORK UNIT NUMBER

7. PERFORMING ORGANIZATION NAMES(S) AND ADDRESS(S)
Air Force Institute of Technology
Graduate School of Engineering and Management (AFIT/EN)
2950 Hobson Way
WPAFB OH 45433-7765

8. PERFORMING ORGANIZATION REPORT NUMBER

AFIT/GAP/ENP/06-14

9. SPONSORING/MONITORING AGENCY NAME(S) AND ADDRESS(ES)
AFWA/DN
Omaha, NE
LtC Trey Cade

10. SPONSOR/MONITOR'S ACRONYM(S)

11. SPONSOR/MONITOR'S REPORT NUMBER(S)

12. DISTRIBUTION/AVAILABILITY STATEMENT
APPROVED FOR PUBLIC RELEASE; DISTRIBUTION UNLIMITED.

13. SUPPLEMENTARY NOTES

14. ABSTRACT

This research takes an existing ionospheric model and modifies it to include the effects of solar flare activity. Solar flares are a localized explosive release of magnetic energy that appears as a sudden, short-lived brightening in the sun's chromosphere. This additional energy is deposited in the earth's ionosphere, temporarily changing its properties, which can affect military communications. Studying the effects of moderate solar flares will improve our understanding of the ionosphere's response, leading to better operational models. Modification of the model is accomplished by adding a flare irradiance model to represent solar irradiance changes due to a flare. The irradiance output is then used to calculate the photoionization rates, electron impact ionization rates, and electron heating rates in the ionospheric model. After the results of this integration are validated, two moderate flares are modeled and then compared to ionospheric measurements from Bear Lake Observatory. It is found that the new model is able to accurately reflect the response of the E and lower F region of the ionosphere, but above the F_2 peak the electron temperature does not increase as initially expected. Future work will need to resolve this discrepancy so that the model can accurately develop the ionosphere's response to solar flares.

15. SUBJECT TERMS
Ionosphere, solar flares, modeling ionosphere

16. SECURITY CLASSIFICATION OF: Unclassified			**17. LIMITATION OF ABSTRACT**	**18. NUMBER OF PAGES**	**19a. NAME OF RESPONSIBLE PERSON**
REPORT	**ABSTRACT**	**c. THIS PAGE**			Christopher G. Smithtro, Maj, USAF (ENP)
U	**U**	**U**	**UU**	75	**19b. TELEPHONE NUMBER** *(Include area code)* (937) 255-3636, ext 4505; e-mail: Christopher.Smithtro@afit.edu

Standard Form 298 (Rev: 8-98)
Prescribed by ANSI Std. Z39-18